



NTNU – Trondheim
Norwegian University of
Science and Technology

Microchannel Membrane Reactor for production of pure Hydrogen

Inhibition effects on thin self-supported
Pd/Ag membranes

Bengt Arild Johannesen

Chemical Engineering and Biotechnology

Submission date: June 2014

Supervisor: Hilde Johnsen Venvik, IKP

Norwegian University of Science and Technology
Department of Chemical Engineering

Preface

This report is written as a part of subject TKP4900 at NTNU in the department of Chemical Engineering, Faculty of Natural Sciences and Technology. The master thesis work consisted of experimental work, which was conducted over the course of 20 weeks, along with literature search and report writing. This was done spring semester 2014.

I would first of all like to thank my supervisor Hilde J. Venvik for the regular follow-up and guidance, as well as showing great enthusiasm for my work. Sincere congratulations and wishes for PhD. Nicola Vicinanza, who gave me invaluable assistance, teachings and company throughout this last year. Thjis Peters (SIN-TEF Materials and Chemistry in Oslo) for providing assistance from afar and providing palladium-silver membranes. Ingeborg-Helene Svenum (Materials and nanotechnology) for helping me handle X-ray photoelectron spectroscopy and its results. I also wish to direct a thank you to Camilla Lindgren for the project collaboration and interesting talks. Finally I would like to thank my fellow students, friends and family for support, laughter and despair over my five years of studies.

I declare that this is an independent work according to the exam regulations of the Norwegian University of Science and Technology (NTNU).

Place and date :
Trondheim, June 12, 2014



Bengt Arild Johannesen

Abstract

Hydrogen gas is one of the most produced gases in the world for industrial purposes, generally produced by methane steam reforming. The demand for clean hydrogen is rising as technology is advancing. Combining a hydrogen separation step with methane steam reforming can be advantageous as pure hydrogen can be produced, total operating cost reduced and CO₂ can possibly be stored. Palladium based membranes have high hydrogen selectivity, solubility and permeability, and are seen as a viable way to purify hydrogen gas from different gas mixtures. This project is investigating the properties of thin self supported Pd/Ag 23wt.% membranes, and CO inhibition effects.

The palladium based membranes were produced by magnetron sputtering, and used in a microchannel membrane setup. The experimental procedure followed several Pd/Ag 23wt.% membranes of 2.2-, 4.7- and 10.0 μ m through different experimental series. Hydrogen permeation, surface characterization, solubility and CO inhibition were investigated.

Hydrogen permeability was observed to increase with temperature. Heat treatment in air at 400°C increased permeability for all membranes and gave a mean value of $1.9 \cdot 10^{-8} \text{ mol m s}^{-1} \text{ m}^{-2} \text{ Pa}^{0.5}$. The hydrogen transport through thin membranes ($\leq 5 \mu\text{m}$) was determined to be limited by surface effects, while thicker ones were governed by bulk diffusion. This was determined by CO inhibition experiment, heat treatment in air and activation energy calculations. Through X-ray photoelectron spectroscopy a silver enrichment was observed on substrate side of all as-grown (unused) membranes, while CO and O species were detected on all membrane surfaces. Hydrogen desorption was suggested as the transport limiting effect. This is due to a reported increase in desorption barriers with increasing Ag content, in association with substrate side silver enrichment.

It was shown that inhibition of hydrogen flux increased with partial pressures of CO and decreasing temperature. Membranes governed by bulk diffusion were less affected by CO inhibition than thinner ones. This was explained by competitive adsorption between CO and H₂ being a surface effect. Heat treatment in air was observed to increase membrane resistance towards inhibitor. Heat treatment before CO exposure was determined to give a significantly better performance of membrane properties. Whereas a membrane already exposed to CO over several experiments was not enhanced after heat treatment in air. CO inhibition led to both irreversible and reversible deactivation, the latter being dominant over short term CO exposure. Irreversible was predominant at lower temperatures, higher CO concentrations and at longer exposure times. After a series of experiments, 4.7 μ m membranes with- and without heat treatment in air had a final flux of 67- and 87%, relative to initial flux. This shows that heat treatment in air procedure increases resistance to CO and valuable lifetime is possibly gained.

Sammendrag

Hydrogengass er en av de mest produserte gassene i verden for industrielle formål, vanligvis fremstilt ved dampreforming av metan. Etterspørselen av ren hydrogen er i takt med dagens rasktvoksende teknologi. Kombinering av hydrogenseparasjon sammen med metan dampreforming kan gi store fordeler som f.eks. produksjon av ren hydrogen gass, reduksjon av de totale driftskostnadene, og muligheten for CO₂-lagring. Palladium baserte membraner har høy selektivitet, løselighet og permeabilitet av hydrogen, og blir sett på som en gunstig måte å rense hydrogengass fra ulike gassblandinger. Dette prosjektet undersøker egenskapene til tynne selvstøttet Pd/Ag23wt.% membraner, og den inhiberende effekten av CO.

Palladium-baserte membraner ble fremstilt ved magneton sputtering, og ble brukt i en mikrokanal-membran konfigurasjon. Eksperimentell prosedyre brukte flere Pd/Ag23wt.% membraner med tykkelse på 2.2-, 4.7- og 10,0 μm gjennom ulike eksperimentelle serier. Hydrogen permeabilitet, overflatekarakterisering, løselighet og CO inhibering ble undersøkt i dette arbeidet.

Hydrogen permeabilitet ble observert å øke med økende temperatur. Varmebehandling i luft ved 400° C økte permeabilitet for alle membraner og ga en gjennomsnittlig verdi på $1,9 \cdot 10^{-8} \text{ mol m s}^{-1} \text{ m}^{-2} \text{ Pa}^{-0,5}$. Hydrogen transport gjennom tynne membraner ($\leq 5 \mu\text{m}$) ble bestemt til å være begrenset av overflateeffekter, mens tykkere membraner ble styrt av bulk diffusjon. Dette ble bestemt ved permeabilitetsmålinger ved tilstedeværelse av CO, varmebehandling i luft og beregning av aktiveringsenergier. Gjennom X-ray fotoelektron spektroskopi ble en berikelse av sølv observert på substratsiden av alle ubrukte membraner, mens CO og O, ble påvist på alle membranoverflater. Hydrogen desorbering ble foreslått som den begrensende faktor for hydrogentransport gjennom membran. Dette skyldes en rapportert økning i desorberingsbarrierer med økende sølvinnhold, samtidig som det ble sett en anrikning av sølv på substratsiden der desorbering skjer.

Det ble vist at inhibering av hydrogenfluks øker med partialtrykk av CO og avtagende temperatur. Membraner styrt av bulk diffusjon ble mindre påvirket av CO enn tynne. Dette ble forklart ved at konkurrerende adsorpsjon mellom CO og H₂ er en overflate effekt. Varmebehandling i luft ble observert til å øke membranens resistens mot deaktivering. Varmebehandling før CO eksponering ble bestemt til å gi en betydelig bedre ytelse av membranegenskapene. Mens en membran som allerede er utsatt for CO i løpet av flere forsøk ikke var forbedret etter varmebehandling i luft. CO inhibering førte til både irreversibel og reversibel deaktivering, sistnevnte er dominerende over kort sikt CO eksponering. Irreversibel deaktivering var dominerende ved lavere temperaturer, høye CO-konsentrasjoner og ved lengre eksponeringstider. Etter en serie eksperimenter ble to membraner av 4,7 μm tykkelse, med- og uten varmebehandling i luft en endelig fluks på 67- og 87%, relativt til initiell. Dette viser at varmebehandling i luft øker resistens mot CO og kan muligens gi økt levetid for membranen.

Contents

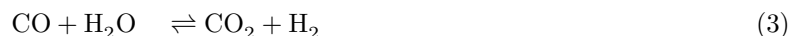
Contents	7
1 Introduction	9
1.1 Motivation	9
1.2 Scope of work	9
2 Theory	11
2.1 Palladium based membranes	11
2.1.1 Transport mechanism	11
2.1.2 Palladium-silver alloy	12
2.1.3 Adsorption modelling	13
2.2 Heat treatment in air	14
2.3 Volumetric equilibrium sorption	14
2.4 X-ray Photoelectron Spectroscopy	17
2.4.1 Principle of X-ray Photoelectron Spectroscopy	17
2.4.2 Analysis and Spectra fitting	19
3 Experimental	21
3.1 Risk analysis	21
3.2 Preperation of membrane and reactor	21
3.3 Permeation experiments	22
3.3.1 Stabilization of hydrogen flux	23
3.3.2 Short term exposure of CO on a Pd/Ag membrane	24
3.3.3 Short term exposure of CO on a used HTA Pd/Ag membrane	24
3.3.4 Short term exposure of CO on a unused HTA Pd/Ag membrane	24
3.3.5 Long term exposure of CO on a Pd/Ag membrane	24
3.3.6 CO exposure on a Pd/Ag membrane without transmembrane pressure difference	24
3.3.7 CO and H ₂ O inhibition effect on different membrane thickness	25
3.4 Sorption measurements	25
3.5 Surface investigation by X-ray photoelectron spectroscopy	26
4 Results	29
4.1 Membrane performance	29
4.1.1 Hydrogen- permeability and permeance of membranes	29
4.1.2 Solubility, diffusivity and activation energy of membranes	30
4.2 CO exposure experiments	33
4.2.1 CO inhibition as a function of temperature, heat treatment in air and CO concentration	33
4.2.2 Heat treatment effect before and after CO exposure	35
4.2.3 Long term exposure of CO on a Pd/Ag membrane	35
4.2.4 CO inhibition effect on different membrane thickness	36

4.3	CO and H ₂ O inhibition effect on different membrane thickness	37
4.4	Deactivation and regeneration of Pd/Ag membrane	38
4.5	Surface investigation by X-ray photoelectron sepectroscopy	39
4.5.1	Spectra	40
4.5.2	Quantification	44
5	Discussion	47
5.1	Pd/Ag membrane properties	47
5.2	The inhibiting effect of CO on Pd/Ag membrane	49
5.3	Surface investigation by X-ray photoelectron spectroscopy	52
6	Conclusion and further work	55
7	References	57

1 Introduction

1.1 Motivation

Hydrogen gas is one of the most produced gases in the world for industrial purposes, with applications such as petroleum hydrogenation, crude oil upgrading, chemical processes, rocket- and general fuel. Generally methane steam reforming (MSR) is seen as a viable way to produce hydrogen gas, as it has a high H:C ratio, low reforming temperatures and can utilize biomass or natural gas as feedstock. The MSR reaction's main products are H₂ and CO₂, and CO due to the water gas shift reaction (WGSR), as well as decomposition of methane [1]. The MSR-, methane decomposition- and WGS reactions are given in Equation 1 - 3. Because of the byproducts in the hydrogen production process the hydrogen gas needs to be purified in order to be utilized by the given processes. Membrane separation is a promising alternative method of hydrogen purification. The proton exchange membrane (PEM) fuel cell is an alternative to the conventional combustion engine, but can not utilize hydrogen gas containing more than ~ 10 ppm CO before electrodes deactivate [2]. Palladium (Pd) metal membranes can be used in the separation process because of their high/total selectivity towards hydrogen, as well as high- permeation and solubility of hydrogen.



A combination of a hydrogen separation and MSR reactions in one catalytic membrane reactor can prove to be advantageous. Total operating cost can be reduced as operating- pressures and temperatures are limited to one compact reactor, where both processes are in the same temperature range of 300-500°C [3]. Equilibrium shift to product side in steam reforming is expected as hydrogen is removed from mixture, facilitating more product conversion, and retention of CO₂ can possibly be integrated with carbon capture in future. Disadvantages with the process is the high palladium cost, compression requirements after a low pressure process and membrane deactivation upon CO and sulphur exposure. The membrane will in addition be exposed to other components from gas mixture, such as CO₂, CH₄, N₂ and H₂O.

1.2 Scope of work

This work is a continuation of a project work, fall 2013 at NTNU, investigating permeation of hydrogen on Pd/Ag 23wt.% membranes, and the inhibiting effect of CO. Membranes were provided by SINTEF Materials and Chemistry in Oslo, and this study has reproduced some of the experiments conducted previously [4, 5] to compare performance of the palladium based membranes, and to further examine their properties. Membrane properties were determined by volumetric sorption technique and permeation experiments. Further, inhibition-, deactivation- and regeneration of hydrogen flux was examined with CO and H₂O in feed mixture to closer simulate industrial process conditions. All permeation measurements through Pd/Ag membranes were done in a microchannel membrane configuration on experimental rig. The responsibility of set-up design required continuous upgrades and changes e.g. piping, process control, equipment, software etc. Surface investigations were performed by X-ray photoelectron spectroscopy (XPS) on both used and unused

membranes to consider what deactivation effects were present.

2 Theory

2.1 Palladium based membranes

2.1.1 Transport mechanism

Palladium membranes have an exceptional selectivity towards hydrogen, as well as high hydrogen permeance and hydrogen solubility, and it is recognized for its high potential for hydrogen separation [6]. The permeation of hydrogen shown in Figure 1 follows a solution diffusion mechanism, consisting of the following steps [7]:

1. Gas diffusion to membrane surface (Feed side)
2. Dissociative adsorption of hydrogen molecule
3. Transport of hydrogen atoms from surface to membrane bulk
4. Atomic diffusion through bulk
5. Transport of hydrogen atoms from membrane bulk to surface
6. Associative desorption of hydrogen atoms
7. Gas diffusion from membrane to surface (Permeate side)

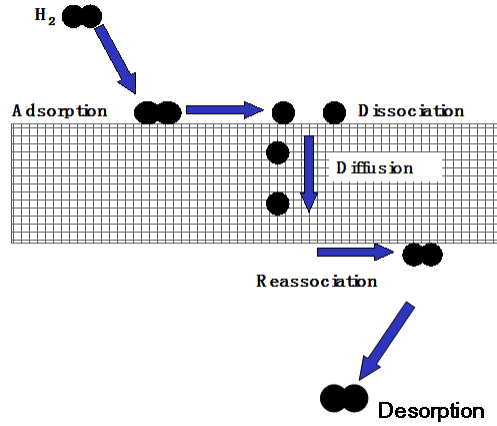


Figure 1: Solution diffusion mechanism on a Pd/Ag 23wt.% membrane. [4, 8]

The hydrogen flux through the palladium-silver membrane, J_{H_2} , can be expressed by Equation 4 and 5.

$$J_{H_2} = \frac{P}{t}(p_1^n - p_2^n) = \frac{K_S D}{t}(p_1^n - p_2^n) \quad (4)$$

$$D = D_0 \exp[-E_a/RT] \quad (5)$$

Where P is the permability of the membrane, t is the membrane thickness, p_1 and p_2 are the partial pressures of hydrogen on high- and low pressure sides respectively, K_S is the solubility constant, D is the diffusion

coefficient, D_0 is a pre-exponential factor, and E_a is the activation energy for the diffusion. P/t is defined as permeance, and is used instead of permeability when the thickness of the membrane is unknown or difficult to accurately measure [4]. The limiting step of the transport mechanism determines the n -value, this is called the rate determining step (rds). Diffusion of hydrogen atoms through the membrane bulk is often a rds when the membrane thickness is high, and the n -value is in these cases $n = 0.5$, following Sieverts' law [7, 9–11]. Hurlbert and Konecny showed that surface reactions were not the limiting step for hydrogen permeability through pure Palladium membranes of 20-150 μm [11]. For thin membranes the diffusion through the membrane bulk is faster, making other processes rds, such as external mass transfer or adsorption/desorption. When the permeation is determined by surface processes, n approaches 1 [7, 9, 10]. Depending on the diffusion through bulk and the external mass transfer, a concentration gradient may occur at the boundary layer at the membrane surface. If permeability is high, and the membrane bulk diffusion is fast there might be diffusion limitations from gas phase to membrane surface. If permeability is low or hindered, the pressure driven process can create an abundance of hydrogen at the surface [12].

Hydrogen permeation through a palladium based membrane follows a solution-diffusion mechanism, where permeability dependent on diffusivity and solubility as shown in Equation 6

$$P = D \cdot K_S \quad (6)$$

where P is permeability of the membrane, D is diffusivity expressed in Equation 5 and K_S is the solubility, also known as the Sieverts' Constant, giving the amount of atomic hydrogen on metal. Sieverts' law explains how the solubility is proportional to the partial pressure of hydrogen at constant temperature, with the assumption that there is no atomic interaction in the dilute hydrogen solution on the metal [13]. This law's deviations have been determined to be at temperatures lower than 250°C and H:Pd ratios of more than 0.006 according to Burch and Francis [14]. Evans reported another deviation, where the law is invalid at pressures above 13.33 kPa due to increased concentration of absorbed hydrogen in palladium [15]. Diffusivity and solubility of hydrogen are both dependent on temperature in a palladium system, as shown in Equation 7 where the Sieverts' constant is expressed as a function of temperature [16].

$$\ln K_S = -\frac{\Delta H_0}{RT} + \frac{\Delta S_0}{R} \quad (7)$$

where ΔH_0 is the solution enthalpy, ΔS_0 is the solution entropy and R is the gas constant. Equation 7 indicates that the solubility decreases with temperature.

2.1.2 Palladium-silver alloy

Many different palladium alloys have been tested, but the Pd/Ag alloy is by far the most investigated alloy. One advantage with a palladium-silver alloy is the reduced production cost, as silver is less expensive compared to palladium. Solubility has been reported to increase with silver content until a maximum at 20-40%, whereas the diffusivity decreases [16, 17]. In addition to providing a decent mechanical stability with 23% wt. silver, it provides high permeability [18]. The permeability value of a Pd/Ag alloy is ~ 1.7 times as high as the permeability value of pure Pd, reported at 350°C [19].

Below the critical temperature there are several phases in which pure palladium will exist. These phases are

called α , $\alpha + \beta$ and β , and depends on the hydrogen concentration, temperature and pressure. The α - *phase* is a denser phase compared to the β - *phase* which is more expanded, meaning the co-existing phase will cause severe strain and distortion to the metal [20]. The phase transition must therefore be suppressed to keep a stable material. This can be done by keeping the temperature and pressure fairly high ($\sim 300^\circ\text{C}$, ~ 2 MPa) [8, 20], or by alloying with other metals. The phases and the transition is described in the hydrogen pressure-composition isotherm for pure palladium, and is given in Figure 2. Alloy studies on the palladium shows that silver as an alloy with palladium lowered the critical temperature, suppressing the undesired phase transition, as well as increasing the permability of hydrogen [21].

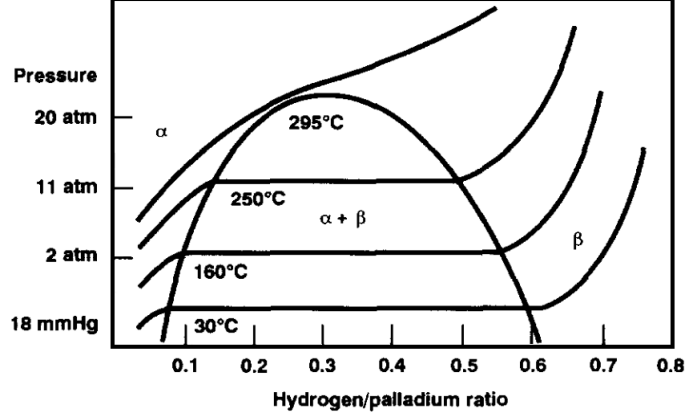
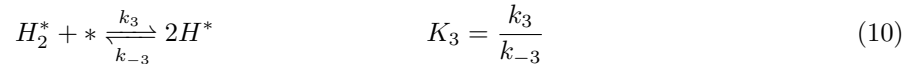
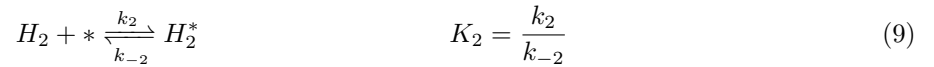
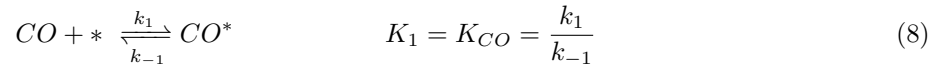


Figure 2: Hydrogen pressure-composition isotherms in pure palladium [8]

2.1.3 Adsorption modelling

A challenge with the PEM fuel cells is the deactivation of electrodes by CO, as it is generally present in the MSR produced hydrogen. The CO is reported to reversibly adsorb onto the palladium surface competitively with H_2 [22–24]. The adsorption of CO will hinder dissociative adsorption of H_2 , and decrease the flux through membrane. Additionally it has been reported that one single CO molecule can take up more than one vacant site on the palladium surface [25]. CO will increase the activation barrier of H_2 's dissociative adsorption and the desorption energy [26]. The three elementary reactions 8 - 10 below describe the adsorption of CO and H_2 onto the palladium surface.



The overall dissociative adsorption of H_2 is given in Equation 11



Where:

$$K = K_{H_2} = K_2 K_3 \quad (12)$$

And the equilibrium constants can be expressed by Arrhenius equation:

$$k_i^{+/-} = A_i \exp[-E_i^{+/-}/RT] \quad (13)$$

With the modelling done from Equation 8 to 13, a Landmuir expression for the competitive adsorption of CO and H₂ on the membrane surface can be made, and is given in Equation 14.

$$\theta_{CO} = \frac{K_{CO} p_{CO}}{1 + K_{CO} p_{CO} + \sqrt{K_{H_2} p_{H_2}}} \quad (14)$$

According to the Equation the CO coverage is highly dependent on partial pressures of CO, as well as temperature dependence and partial pressure of H₂. The partial pressure of CO highly determines the CO coverage of the surface, as well as partial pressure of H₂ and temperature [24].

2.2 Heat treatment in air

It has been reported that hydrogen permeation of a palladium membrane can be improved by heat treatment in air (HTA), where it is exposed to oxygen at elevated temperatures and forms an oxide layer [27], which is subsequently reduced [28–34]. Hydrogen permeation is found to double in some cases when the treatment is performed on thin membranes [28, 31, 35, 36]. There are three main hypothesis that describes the effect behind HTA: Surface roughening, Pd segregation to surface and cleaning of surface. Mejdell et al. investigated the effect of CO inhibition on a palladium-silver membrane before and after heat treatment in air, and determined that CO inhibition was significantly reduced by HTA [35]. The study suggests that the HTA has a positive effect on CO inhibition because of an alternation in membrane structure and the surface's electronic properties, caused by the oxidation and subsequent reduction. Vicinanza et al. concludes that heat treatment increases surface roughness and permeability through increased diffusivity, while hydrogen solubility is unaffected [37]. Increased surface roughness will give a larger effective surface area, yielding higher permeation of hydrogen. Theoretical electronic ground state predictions have found palladium atoms to strongly segregate to membrane surface upon surface oxidation at elevated temperatures [38], possibly increasing permeability due to a minimum hydrogen adsorption barrier to palladium [39]. In addition, heat treatment in air is reported to recover the Pd based membrane after poisoning and deactivation effects [40, 41].

2.3 Volumetric equilibrium sorption

The solubility of hydrogen in metals can be done by several methods, such as: volumetric- [32] and gravimetric absorption, sample dilation, electrical resistance and temperature programmed desorption. However, with common and conventional technology volumetric and gravimetric absorption is by far the most used, and gives comparable results even though volumetric is a volume/pressure analysis and gravimetric is based on

mass measurements. In this work ad-/absorption of light hydrogen gas is investigated on palladium metals, hence the volumetric analysis is utilized due to the low mass of hydrogen molecules.

The volumetric sorption analysis is a relatively easy investigation where volume changes are detected as ad-/absorption of hydrogen onto the metal occurs, at known temperature and pressure. This analysis is also called the *manometric* (Sieverts) method, and the set-up is shown in Figure 3.

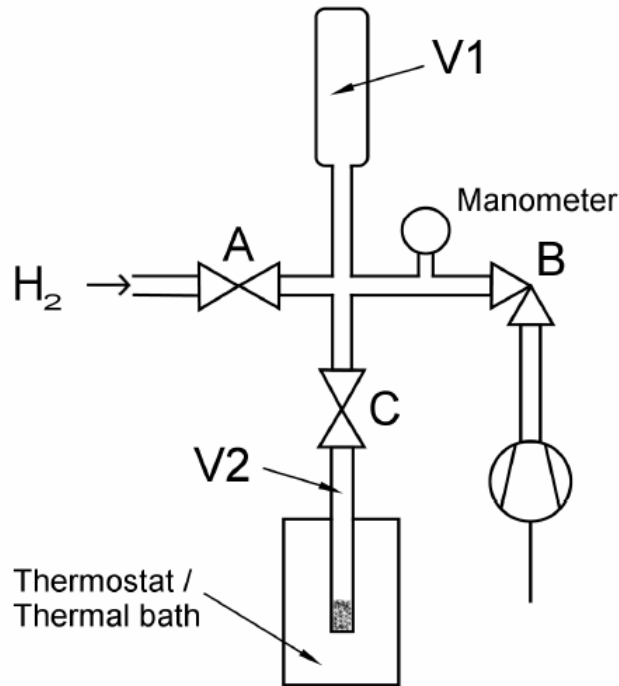


Figure 3: Schematic illustration of volumetric sorption technique, the manometric method [42].

Figure 3 shows the schematic of a volumetric sorption set-up where V_1 and V_2 are the known volumes of the reservoir- and sample tube respectively, A -valve controls the flow of hydrogen in, valve C controls the flow in and out of sample tube, V_2 , and valve B controls the outflow and vacuum of the set-up. The dead volume of the sample tube is measured with inerts before any measurements. Both V_1 and V_2 are evacuated by opening valves C and B , and at desired vacuum they are closed and hydrogen gas is introduced through valve A . When closing valve A the initial pressure, P_i in V_1 will be measured by the manometer, and by opening valve C the sample will be exposed to H_2 . The pressure will drop as hydrogen gas in V_1 fills $V_1 + V_2$. The final pressure, P_f is recorded at equilibrium between hydrogen in gas phase and on the metal, at a specific hydrogen partial pressure and temperature. The final amount of hydrogen absorbed on sample is calculated through the universal gas law, where the final hydrogen uptake is expressed as the difference of hydrogen in reservoir and gas phase at end: $\Delta n = n_i - n_f$. The universal gas law is given in Equation 15

$$\Delta n = \frac{P_i V_1}{RT} - \frac{P_f (V_1 + V_2)}{RT} \quad (15)$$

where T is the temperature and R is the gas constant. The described process is repeated with subsequent gas expansions for increasing P_i in order to generate the isotherm results.

2.4 X-ray Photoelectron Spectroscopy

2.4.1 Principle of X-ray Photoelectron Spectroscopy

X-ray Photoelectron Spectroscopy is a common experimental technique for investigation of surface composition and properties. The technique is based on the photoelectric principle, where a material surface emits electrons when hit by photons. H. Hertz made this discovery in 1887 [43], and A. Einstein later explained the phenomenon, awarding him the Nobel prize (1921) [44]. K. Siegbahn and his fellow researchers at University of Uppsala developed the X-ray Photoelectron Spectroscopy technique in 1950-1970 [45]. K. Siegbahn was awarded the Nobel prize in physics in 1981 based on this work.

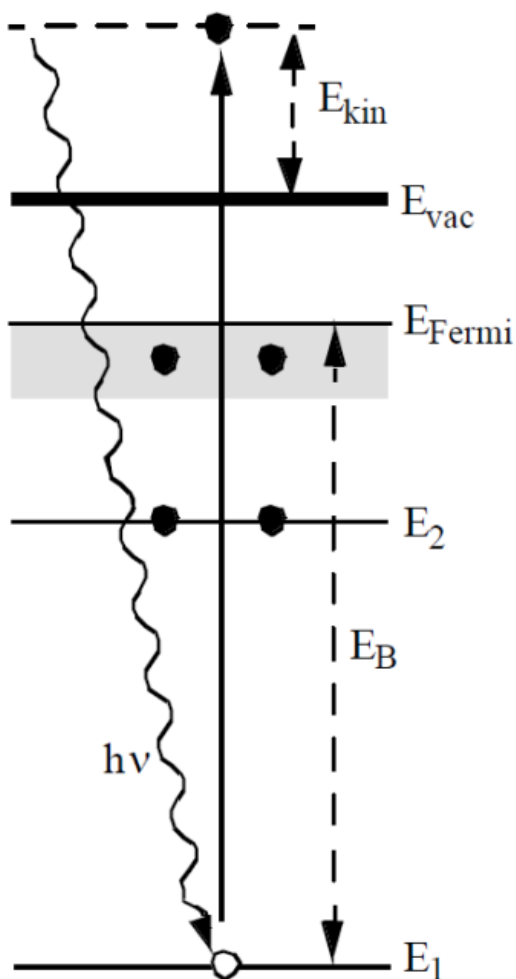


Figure 4: Schematic of the XPS principle [46].

In Figure 4 the photon emission principle and its energy levels are shown for XPS. The energy conservation when a sample is irradiated by light can be expressed as

$$E_{kin} = h\nu - E_B + \Phi_S \quad (16)$$

where $h\nu$ is the energy of the incoming photon that excites the core electron at E_B relative to the fermi level, E_f , E_{kin} is the energy of the emitted electron from the surface, Φ_S is the energy required for the electron to get to the vacuum level, E_{vac} from E_f . In order to have a photoemission effect the incoming photon must be of sufficient energy for the electron to overcome its binding energy E_B and the work function of the sample Φ_S . The kinetic energy can be expressed with ionizing potential, which is the energy difference in final and initial state energies of the system

$$E_{in} + h\nu = E_{fin} + E_{kin} \quad (17)$$

where E_{in} and E_{fin} are the initial and final state energies of the system.

The binding energy of the emitted electrons is obtained by measuring the kinetic energy distribution of the emitted photoelectrons.

The core electron of an element has an unique and characteristic binding energy, which enables identification of specific elements and chemical environments by surface investigation with XPS. The intensity of the core levels are used to quantify the amount of specific element on the surface. Figure 5 shows a typical XPS spectrum with intensity (here expressed as no. of electrons) against the binding energy, eV .

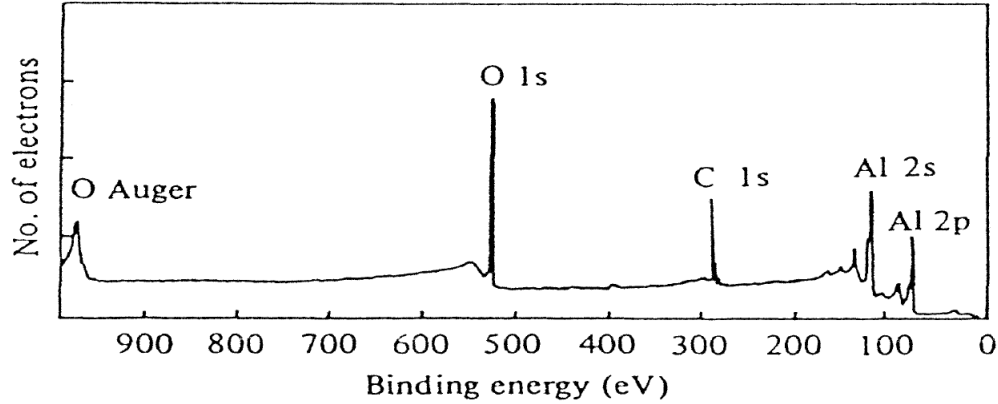


Figure 5: A typical XPS spectrum of an Al metal [47].

The spectrum shows an oxidized Al metal with carbon contaminants, and it gives both quantitative and qualitative information on components present on the surface. The amount is indicated through the area of the peak, whereas the shape and binding energy indicates the specific element and its state. Recognizable peaks in this spectrum are: O 1s, C 1s, Al 2s and Al 2p, as well as the O Auger peak. Photons are commonly provided by X-ray sources such as Al $K\alpha$ (1486.6 eV) and Mg $K\alpha$ (1253.6 eV). The Auger emission peaks, E_{kin} , are independent on the photon energy, $h\nu$, making it distinguishable when the photon source is varied. Tunable photon energy can be done by non-conventional synchrotron radiation sources, and provides further investigation opportunities. Each element has an unique length at which the electron can travel through a solid without loss of energy, this is called the inelastic electron mean free path [47, 48], an overview for several elements is given in Figure 6. Synchrotron photon sources may therefore be tuned to change the surface sensitivity of detection. This opens up for investigations of bulk and surface contributions in the spectra. Thus, the case where the photon sources cannot be tuned, the background of inelastic electrons cannot be varied. The valence level spectra, here seen close to $E_B=0$ has an analytical value, but does not significantly contribute to this work, hence not discussed any further.

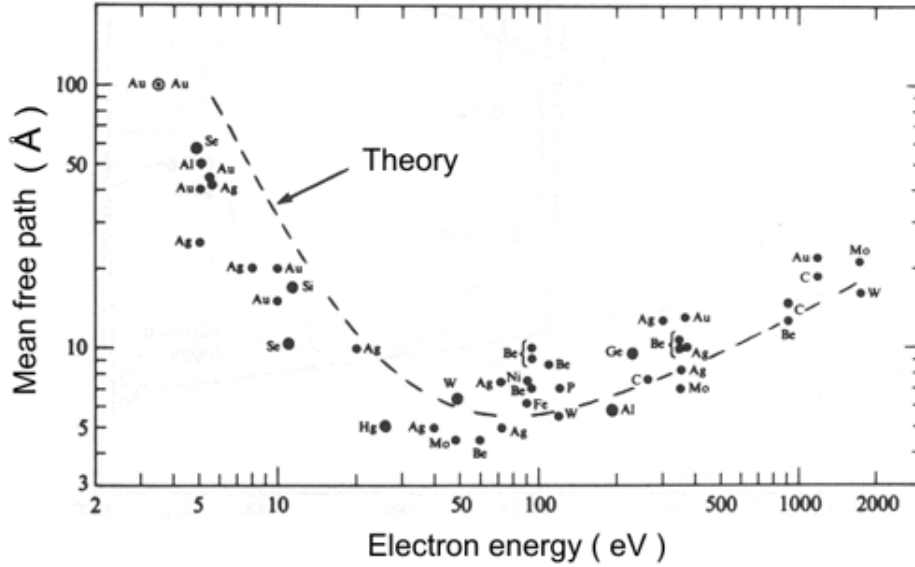


Figure 6: The electron mean free path, Å, against the electron energy, eV, for several elements [48, 49]. Stippled line indicates the theoretical calculations done by Penn [50]

2.4.2 Analysis and Spectra fitting

Identification of elements is done using databases and literature tables of element's specific binding energy. Further analysis of a photoelectron spectra is generally done by curve fitting, with the assumption that every photoelectron peak is represented by parameters describing its binding energy, area and line shape. Lorentzian and Gaussian functions are commonly used when describing line shapes, along with an asymmetric factor. These are applied for the detailed quantification and analysis of chemical environment. The precision depends on the cross section (signal) from the core-level and the instrumental resolution of the equipment. Generally, high intensity photon, coherent photon sources and advanced photon detectors enable high resolution. Background contributions due to inelastic electrons must be subtracted in order to estimate the peak intensity and for quantification purposes. Linear or Shirley backgrounds are a commonly used for this subtraction, the latter is based on the assumption that the intensity of inelastic electrons at E_B is proportional to the integrated intensity of peak at E_B (minus the background), as shown in Equation 18.

$$I_B(E) \propto \int_{E_0}^E (I(E) - I_B(E)) dE \quad (18)$$

Where I_B is the intensity of inelastic electrons, E_0 and E is the low- and high energy side of the photoemission peak respectively, and I is the intensity of the peak.

3 Experimental

3.1 Risk analysis

Risks associated with experimental laboratory work were evaluated, and the risk assessments are given Appendix A. Overall, leakage, fire and exposure to toxic and flammable substances (CO, H₂) were determined to be the highest likelihood of instance, and highest risk in this work. Continuous leak testing before and during experiments were performed to avoid these instances. Experimental rig had CH₄ and CO detectors installed, both cross detecting H₂. In addition the pipes were checked with soap solution at inert flow. Hand held H₂ detector(Cross detecting CO) were used with hydrogen gas on stream. During permeation experiments the pressure was monitored, as a pressure drop might indicate a leak in the system.

3.2 Preperation of membrane and reactor

A thin self-supported Pd/Ag 23wt.% membrane was provided by SINTEF Oslo, which was produced by a two-step magnetron sputtering process onto a silicon wafer [51]. The microchannel configuration consisted of: a channel housing, membrane, perforated plate, copper gasket and a permeate housing. The seven feed channels corresponded to an active surface area of 0.91cm^2 . The microchannel configuration shown in Figure 7 was first polished by silicon carbide grinding paper of the grits 1200, 2500 and 4000, in respective order. Polishing was done in the presence of water at 150rpm, until a clear surface was observed. The copper gasket was only polished with a grit of 2500, to ensure a efficient sealing. The configuration was cleaned by submerging the pieces in ethanol in an ultrasonic cleaner for 10 minutes. Configuration pieces was dried both externally and internally by compressed air, followed by compressed argon. The membrane was cut in an appropriate size by both stanley knife and a scalpel. By the means of regular scotch tape, the membrane was lifted from the wafer and onto the perforated plate, ontop of the permeate housing and the copper gasket. Growth side of membrane was placed facing the feed/retentate side, wheras substrate side faced the permeate/sweep side. Holes were punched through the membrane by using a copper wire, indicating the position of screws. The channel housing was placed on top, and fastened with an alternated tightening of the screws, to not strain the membrane. Excess membrane was cut off and put in a bottle as residue. A detailed mounting procedure is given in Appendix B.

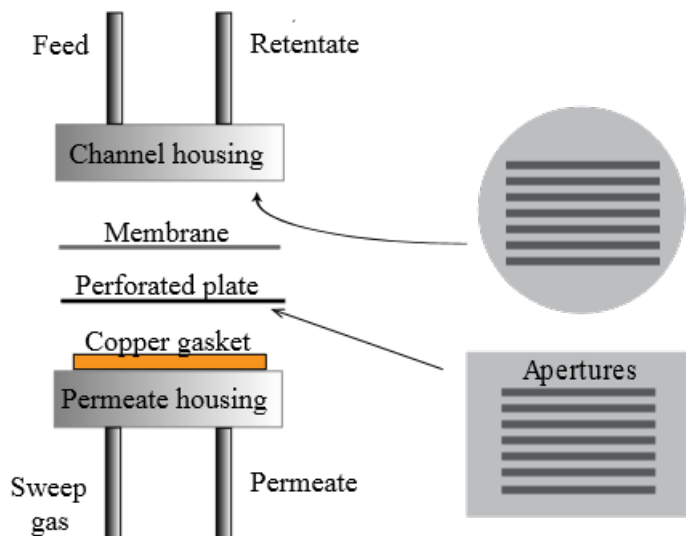


Figure 7: Microchannel parts and configuration

3.3 Permeation experiments

All experiments performed are listed in order of time performed in Table 1, along with their main parameters. Experiments 1a-3d were done with a feed side total pressure of 2.2 bar, which was measured and kept constant by a back-pressure controller. Experiment 4a-6c were done without any pressure control and $\sim \Delta P = 0$ over the membrane. During experiments the total volumetric gas flow was kept at 400 NmL/min by the use of a series of mass flow controllers (MFC). Gas velocity was kept high in order to avoid concentration profiles along the membranes, and to eliminate mass transfer limitation from gas bulk to surface. MFC Calibrations are given in Appendix C. A Micro-GC was used in order to check and detect leakages through membrane. Calibration of Micro-GC is given in Appendix D.

The reactor was ramped to the initial temperature with nitrogen and argon on stream, on feed side and permeate side respectively, ramping at $2^\circ\text{C}/\text{min}$. Hydrogen was not introduced to the system before 300°C was reached, in order to suppress phase transition of the palladium-silver material. The membrane was stabilized with a hydrogen:nitrogen mix of 9:1. Permeability and permeance was calculated from the permeate flow, measured using a bubble flow meter or a micro-GC. The hydrogen concentration was kept at 90 % for all experiments, and remaining 10% consisted of N_2 and CO. CO concentrations varied in the range of 0-5.0 % depending on type of investigation. The amount of N_2 correlated to CO, giving a total feed flow of 400NmL/min. CO was introduced in stream when membrane flux had stabilized. Experiment 1a-3d have a constant CO concentration throughout, whereas experiment 4a-6c has an increasing CO concentration over time. The membrane reactor set up flow sheet is given in Appendix E.

Table 1: Order of experiments done, and their main parameters

Experiment	Thickness [μm]	Temperature [$^{\circ}C$]	CO Concentration [%]	HTA	ΔP [Bar]
1a	~ 2.2	300	0.5 %	no	1
2a	~ 4.7	400	0.5 %	no	1.2
2b	~ 4.7	400	2.0 %	no	1.2
2c	~ 4.7	350	0.5 %	no	1.2
2d	~ 4.7	350	2.0 %	no	1.2
2e	~ 4.7	300	0.5 %	no	1.2
2f	~ 4.7	300	2.0 %	no	1.2
3a	~ 4.7	400	0.5 %	yes	1.2
3b	~ 4.7	400	2.0 %	yes	1.2
3c	~ 4.7	350	0.5 %	yes	1.2
3d	~ 4.7	350	2.0 %	yes	1.2
4a	~ 4.7	400	0.5 %	yes	1.2
4b	~ 4.7	400	2.0 %	yes	1.2
4c	~ 4.7	350	0.5 %	yes	1.2
4d	~ 4.7	350	2.0 %	yes	1.2
4e	~ 4.7	300	0.5 %	yes	1.2
4f	~ 4.7	300	2.0 %	yes	1.2
5a	~ 2.2	300	0-5 %	no	0
5b	~ 2.2	400	0-5 %	yes	0
5c	~ 2.2	300	0-5 %	yes	0
6a	~ 4.7	300	0-5 %	no	0
6b	~ 4.7	400	0-5 %	yes	0
6c	~ 4.7	300	0-5 %	yes	0
7a	~ 10.0	300	0-5 %	no	0
7b	~ 10.0	400	0-5 %	yes	0
7c	~ 10.0	300	0-5 %	yes	0
8a	~ 10.0	300	0-4% CO + 0-4% H ₂ O	yes	0
8b	~ 2.2	300	0-2% CO + 0-4% H ₂ O	yes	0

Note that in the experimental series of 2 and 3 the same membrane was used, but the membrane underwent HTA before series 3 started. Appendix F shows the flux of the 4.7 μm non-HTA membrane over experiments 2a-2f.

3.3.1 Stabilization of hydrogen flux

Before starting any CO exposure experiment the stabilization of hydrogen flux was monitored. The standard routine for a membrane-gas phase equilibrium check, was to monitor the hydrogen flux. The flux was considered stable when measurements were approximately constant over time.

3.3.2 Short term exposure of CO on a Pd/Ag membrane

Inhibition of CO on a 4.7 μm Pd/Ag 23wt.% membrane was investigated over a short time. The stable hydrogen flux was measured at 400°C, 350°C and 300°C, before 0.5% CO was introduced. The flux was closely monitored for 1.5 hours, where 60 minutes consisted of CO exposure and 30 minutes of regeneration in absence of CO. Thereafter the hydrogen flux was loosely monitored until approximately full regeneration of flux under 9:1 $\text{H}_2:\text{N}_2$ (generally over night). The membrane was then introduced to 2.0% CO, and the procedure was repeated. The experiments were done with CO concentrations of 0.5% and 2.0% on the temperatures 400°C, 350°C and 300°C in respective order. The total feed side pressure was kept constant at 2.2bar during the entire experiment. These experiments are labeled 2a-2f in Table 1.

3.3.3 Short term exposure of CO on a used HTA Pd/Ag membrane

After the series of experiments in section 3.3.2, the membrane was left at 400°C for two days. The flux was measured before a heat treatment in air(HTA) at 400°C. The HTA was done by flushing retentate side with 50NmL/min N_2 and the permeate side with 50 NmL/min Ar for 15 minutes. The reactor configuration was then detached in order to expose the membrane to air, and left for an hour at 400°C before an additional N_2 /Ar-flushing for 15 minutes. The flux after HTA was left to stabilize and was measured at the temperatures 400°C, 350°C and 300°C within the scope of one day. The flux was measured again after a day to ensure stable flux. Experiments with exposure to 0.5% and 2.0% CO were done in the same manner as section 3.2.3 at 400° and 350°, with a total feed side pressure of 2.2 bar. These experiments are labeled 3a-3d as shown in Table 1.

3.3.4 Short term exposure of CO on a unused HTA Pd/Ag membrane

The experiments described in section 3.3.3 above were performed following the same procedure with an unused membrane from the same wafer. This was done due to the membrane in section 3.3.3 being exposed to a fair amount of CO, and total regeneration of flux was never complete. The new 4.7 μm Pd/Ag 23wt.% membrane underwent a HTA like section 3.3.3 describes before exposure to any CO. 0.5% and 2.0% CO exposure was done at temperatures of 400°C, 350°C and 300°C. These experiments are labeled 4a-4f in Table 1.

3.3.5 Long term exposure of CO on a Pd/Ag membrane

Inhibition of CO on a 2.2 μm Pd/Ag 23wt.% membrane was investigated over a longer period of time. The hydrogen flux was stabilized at 300°C, before CO was introduced. The gas composition was set to contain 0.5% CO, and the flux was measured irregularly over three consecutive days. Upon CO removal, the membrane regeneration was monitored for two days at 300°C then at 400°C for two days. This experiment is labeled 1a in Table 1.

3.3.6 CO exposure on a Pd/Ag membrane without transmembrane pressure difference

Inhibition of CO on a Pd/Ag 23wt.% membrane was investigated with no transmembrane pressure difference. This was done with membrane thicknesses of 2.2 μm , 4.7 μm and 10.0 μm . Hydrogen flux was stabilized and

measured at 300°C and 400°C. The membrane was exposed to 0.5%, 1.0%, 2.0% and 5.0% CO, for 45 minutes each in increasing order. Hydrogen gas flow on permeate side was measured using a Micro-GC. CO inhibition experiment was done at 300°C, before a HTA. The HTA was done like in section 3.3.3, by flushing retentate side with 50 NmL/min N₂ and the permeate side with 50 NmL/min Ar for 15 minutes. The reactor configuration was detached in order to expose the membrane to air, and left for an hour at 400°C before an additional flushing at 15 minutes. The flux after HTA was left to stabilize and was measured at the temperatures 400°C and 300°C. CO exposure was then done at 400°C followed by complete regeneration of hydrogen flux over night, with the absence of CO. CO inhibition experiment was done again at 300°C, and this procedure was done for the membrane thicknesses. These experiments are labeled 5a-7c in Table 1.

3.3.7 CO and H₂O inhibition effect on different membrane thickness

Inhibition of CO and H₂O on a Pd/Ag 23wt.% membrane was investigated with no transmembrane pressure difference. This was done with membrane thicknesses of 2.2 μm and 10.0 μm. 10.0 μm membrane used in section 3.3.6 was used as hydrogen flux was close to fully regenerated. Membrane of 2.2 μm was taken from a new wafer and mounted. Hydrogen flux was stabilized and measured at 300°C and 400°C, before it was Heat treated in air. The membranes were exposed to 2.0% CO (Only 10.0 μm), then 2.0% CO and 2.0% H₂O, and finally 4.0% CO 4.0% H₂O. Each step was done overnight until hydrogen flux was stabilized. Water was supplied from an installed water tank, under pressure. The liquid flow controller was calibrated by weighing weight at varying set points. The calibration is given in Appendix G. Mettler Toledo XA204 Delta Range Analytical Balance was used to determine the water mass. Hydrogen gas flow on permeate side was measured using a bubble flow meter, and Micro-GC was used to monitor species present in retentate flow. The inhibition experiments were done at 300°C after a Heat treatment in air was performed, like described in section 3.3.3.

3.4 Sorption measurements

The solubility of as-grown Pd/Ag membranes of 2.2 μm, 4.7 μm and 10.0 μm thicknesses were measured using a volumetric sorption technique. Membrane samples were cut from silicon wafer and placed in glass reactor. The sample weight was determined analytically using a Mettler Toledo XA204 Delta Range Analytical Balance, and was aimed to be 0.1 grams for accurate sorption measurements, in addition to have results comparable to that of Vicinanz et al. and Ness. The sorption measurements were conducted using an ASAP 2020 Chemisorption Analyzer (Micrometics Instrument Corporation) with hydrogen partial pressure of 0.02 - 90.66 kPa, and at 300°C, 350°C and 400°C. A degassing procedure was performed prior to any measurements in order to clean sample surfaces. Hydrogen was introduced at 300°C for all samples, in order to avoid phase transition in the Pd/Ag alloy. Helium was present in heating stages to avoid embrittlement of the membrane. All measurements were done twice at the same temperature, and the final sample weight after measurements was determined and used to correct the sorption results. The mass correction was done due to possible reduction in sample mass upon degassing. Table 2 shows the apparatus sequence set in order to perform sorption measurements. The respective sequences done at 350°C and 400°C are given in Appendix H.

Table 2: Apparatus sequence of sorption measurements performed at 300°C.

Task	Gas	Temperature [°C]	Rate [°C/min]	Time [Min]
Evacuation	Helium	100	10	30
Evacuation	Helium	300	10 ¹	15
Evacuation		300	10 ¹	120
Leak test		300	10 ¹	-
Evacuation		300	10 ¹	60
Analysis	Hydrogen	300	10 ¹	-

¹ Temperature rate is given here without stepwise increase in temperature. This is an apparatus setting in order to keep constant temperature.

3.5 Surface investigation by X-ray photoelectron spectroscopy

The membrane thicknesses of 10 μ m, 4.7 μ m and 2.2 μ m, both growth- and substrate side were investigated using X-ray Photoelectron Spectroscopy. The membrane samples were cut from the silicon wafer and attached to a sample plate with carbon tape. Two 4.7 μ m membranes which underwent experiments were investigated on the growth/feed side. The channels of these membranes were cut out of the reactor configuration after experiment 3d and 4f, (Table 1), and placed on sample holder with carbon tape. A survey acquisition was done on all membranes on both sides, with further investigation on the peaks present in the survey. The peak specific acquisition was done with a Hybrid lens mode and a pass energy of 20, with 3-10 sweeps each.

Curve fitting was done using CasaXPS ver.2.3.16, Casa Software Ltd. All fittings were done with a Shirley background. The synthetic line shape used was a Gaussian-Lorentzian function GL(m) where m=0 is pure Gaussian and m=100 is pure Lorentzian, as well as the line shape LA(a,b,n), which is a Lorentzian assymmetric function form convoluted with a Gaussian. The curve fittings of the three key peaks in these spectrums; Pd 3d 5/2, Ag 3d 5/2 and C 1s are given in Figure 8, 9 and 10 respectively. The line shape is displayed as a brown solid line, and the measured data poins are shown as a dashed red line. The complete list of all the curve fittings done is given in Appendix I.

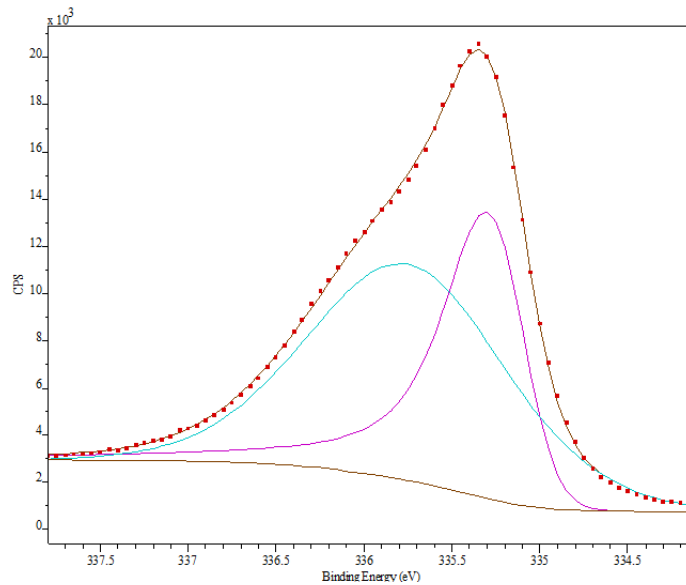


Figure 8: Curve fitting of a Pd 3d 5/2 peak from a XPS spectrum of as-grown 4.7 μ m Pd/Ag membrane

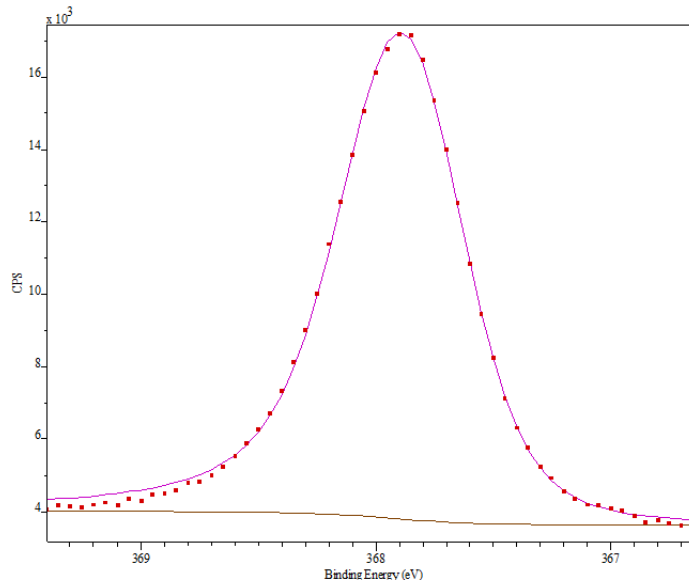


Figure 9: Curve fitting of a Ag 3d 5/2 peak from a XPS spectrum of as-grown 4.7 μ m Pd/Ag membrane

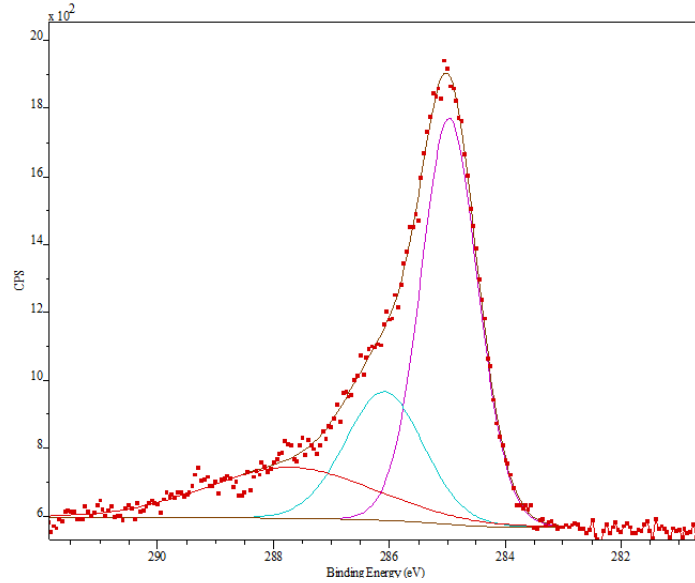


Figure 10: Curve fitting of a C 1s peak from a XPS spectrum of as-grown $4.7\mu\text{m}$ Pd/Ag membrane

Curve fitting of Pd 3d $5/2$ spectrum was made using two components and the same line shape functions for all the samples. Some minor adjustments to the line shape function was done for optimal fitting. Curve fitting of Ag 3d $5/2$ spectrums was possible using one component, with close to identical line shapes. The fitting of C 1s spectrums were done using three or four components, as this was the most varying of the peaks, hence the line shape functions varied accordingly.

Quantifications of surface components were done by calculations on area of the synthetic line shape for Pd 3d $5/2$, Ag 3d $5/2$ and C 1s, for each membrane thickness and side.

4 Results

4.1 Membrane performance

4.1.1 Hydrogen- permeability and permeance of membranes

All membranes investigated in this work were provided by SINTEF Materials and Chemistry. Hydrogen flux through membrane measured at 300°C, 400°C, and on some occasions 350°C. Permeance and permeability were calculated from flux in order to compare with other Pd/Ag 23wt.% membranes provided by SINTEF. A n -value of 0.5 were used in calculations in all the results shown. $n=0.5$ is valid when bulk diffusion is the rate determining step, making the permeability a material constant, and permeance inversely proportional to membrane thickness. The permeance and permeability of membranes used in this work, as well as Pd/Ag membranes investigated by Mejdell et al. and Vicinanza et al. are shown in Table 3, both before and after HTA.

Table 3: Permeance and permeability of Pd/Ag 23wt.% membranes at 300°C, 350°C and 400°C, provided by SINTEF Materials and Chemistry in Oslo.

Thickness [μm]	Temperature [°C]	ΔP_T^1 [bar]	Permeance		Permeability	
			[$mol \cdot m^{-2} \cdot s^{-1} \cdot Pa^{-0.5}$]		[$mol \cdot m \cdot m^{-2} \cdot s^{-1} \cdot Pa^{-0.5}$]	
			no-HTA	HTA	no-HTA	HTA
~ 2.2	300	0	$2.6 \cdot 10^{-3}$	$4.9 \cdot 10^{-3}$	$5.9 \cdot 10^{-9}$	$1.1 \cdot 10^{-8}$
~ 2.2	400	0	$6.2 \cdot 10^{-3}$	$8.2 \cdot 10^{-3}$	$1.4 \cdot 10^{-8}$	$1.8 \cdot 10^{-8}$
~ 2.2	300	1.2	$6.8 \cdot 10^{-3}$	-	$1.5 \cdot 10^{-8}$	-
~ 2.2 [28]	300	0.5	$3.5 \cdot 10^{-3}$	$8.6 \cdot 10^{-3}$	$7.7 \cdot 10^{-9}$	$1.9 \cdot 10^{-8}$
~ 2.2 [28]	300	0.5	$4.6 \cdot 10^{-3}$	$9.2 \cdot 10^{-3}$	$1.0 \cdot 10^{-8}$	$2.0 \cdot 10^{-8}$
~ 2.2 [52]	300	0-1.0	$5.0 \cdot 10^{-3}$	$5.9 \cdot 10^{-3}$	$1.1 \cdot 10^{-8}$	$2.0 \cdot 10^{-8}$
~ 4.7	300	0	$1.3 \cdot 10^{-3}$	$2.6 \cdot 10^{-3}$	$5.9 \cdot 10^{-9}$	$1.2 \cdot 10^{-8}$
~ 4.7	400	0	$2.4 \cdot 10^{-3}$	$4.7 \cdot 10^{-3}$	$1.1 \cdot 10^{-8}$	$2.2 \cdot 10^{-8}$
~ 4.7	300	1.2	$4.8 \cdot 10^{-3}$	$5.2 \cdot 10^{-3}$	$2.3 \cdot 10^{-8}$	$2.4 \cdot 10^{-8}$
~ 4.7	350	1.2	$4.8 \cdot 10^{-3}$	$5.2 \cdot 10^{-3}$	$2.3 \cdot 10^{-8}$	$2.6 \cdot 10^{-8}$
~ 4.7	400	1.2	$5.0 \cdot 10^{-3}$	$5.5 \cdot 10^{-3}$	$2.3 \cdot 10^{-8}$	$2.6 \cdot 10^{-8}$
~ 5.0 [28]	300	0.5	$3.1 \cdot 10^{-3}$	$4.0 \cdot 10^{-3}$	$1.6 \cdot 10^{-8}$	$2.0 \cdot 10^{-8}$
~ 5.0 [28]	300	0.5	$2.7 \cdot 10^{-3}$	$3.9 \cdot 10^{-3}$	$1.4 \cdot 10^{-8}$	$2.0 \cdot 10^{-8}$
~ 4.7 [52]	300	0-1.0	$3.6 \cdot 10^{-3}$	$4.5 \cdot 10^{-3}$	$1.7 \cdot 10^{-8}$	$2.1 \cdot 10^{-8}$
~ 10.0	300	0	$1.4 \cdot 10^{-3}$	$1.2 \cdot 10^{-3}$	$1.4 \cdot 10^{-8}$	$1.2 \cdot 10^{-8}$
~ 10.0	400	0	$1.8 \cdot 10^{-3}$	$1.9 \cdot 10^{-3}$	$1.9 \cdot 10^{-8}$	$1.9 \cdot 10^{-8}$
~ 8.5 [52]	300	0-1.0	$2.5 \cdot 10^{-3}$	$2.6 \cdot 10^{-3}$	$2.1 \cdot 10^{-8}$	$2.2 \cdot 10^{-8}$

¹ Total pressure difference across membrane. With $\Delta P_T \leq 0.5$ bar, sweep gas was used as driving force.

Table 3 shows that the permeation properties of the membranes used in this project generally was lower than others provided by SINTEF Materials and Chemistry, Oslo at 300°C. Only one instance of higher permeation than Mejdell et al. and Vicinanza et al. was observed, which is with an applied transmembrane

pressure difference of 1.2 bar. Although the permeability is a material constant when transport is bulk-limited, it was seen to vary in several cases. Most notable dissimilarity in permeability values was on $4.7\ \mu\text{m}$ membranes, where flux was measured with and without a transmembrane pressure difference. With a pressure difference across the membrane, permeability is observed to be similar for all temperatures tested. This is not the case for membranes where sweep gas was used as driving force instead of pressure difference, where permeability varied with temperature to a larger degree. The permeability value of $2.2\ \mu\text{m}$ membrane utilized in experiment 8b was not included in this table, due to extremely poor performance, and not functioning as a well structured- or clean membrane.

Figure 11 compares permeance as a function of inverse membrane thickness at 300°C and 400°C , for non-HTA and HTA membranes. Permeance was calculated with $n = 0.5$ and $\Delta P = 0$ over the membrane. The stippled line indicates the mean permeance value of $100\ \mu\text{m}$ thick Pd/Ag 23wt.% at 300°C [53].

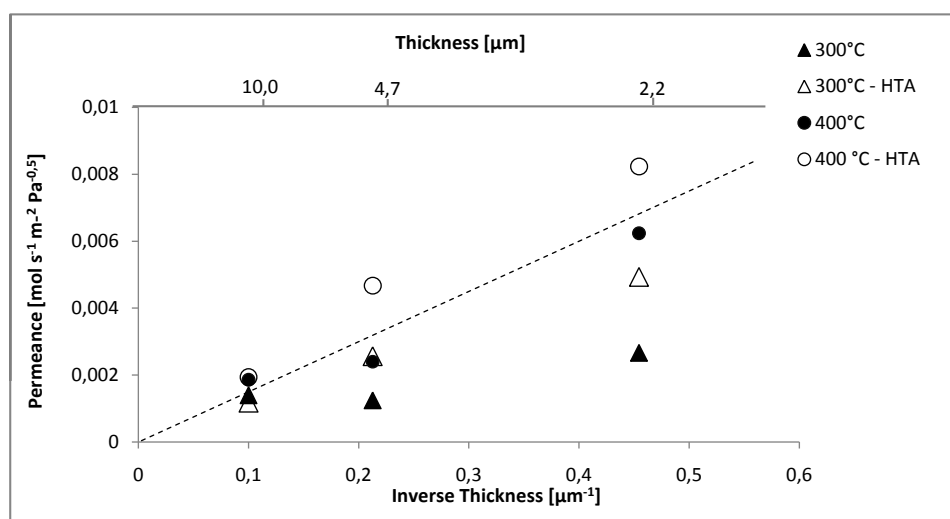


Figure 11: The permeance of palladium based membrane plotted against the inverse thickness, at 300°C and 400°C for samples non-HTA and HTA. Stippled line indicates an average permeability value of $1.5 \cdot 10^{-8} \text{ mol s}^{-1} \text{ m}^{-2} \text{ Pa}^{0.5}$, at 300°C [53].

Figure 11 indicates an increase in permeance with temperature and HTA, and the effect of temperature and HTA on permeance was reduced for thicker membranes, as oppose to thinner ones. The stippled line indicates the permeance of a $100\ \mu\text{m}$ thick membrane at 300°C , where membrane bulk diffusion is assumed to be the transport limiting process. At 300°C it was apparent that permeance values deviate from this line as membrane thickness decreases, and all permeance values of $10\ \mu\text{m}$ show similarity to that of bulk diffusion limitations.

4.1.2 Solubility, diffusivity and activation energy of membranes

Volumetric absorption was used to measure the uptake of hydrogen gas for the palladium-silver alloy at constant temperatures of 300°C , 350°C and 400°C . The hydrogen solubility of a $4.7\ \mu\text{m}$ membrane is provided in Figure 12, while the isotherms for the membrane thicknesses of $2.2\ \mu\text{m}$ and $10.0\ \mu\text{m}$ are given in Appendix

J.

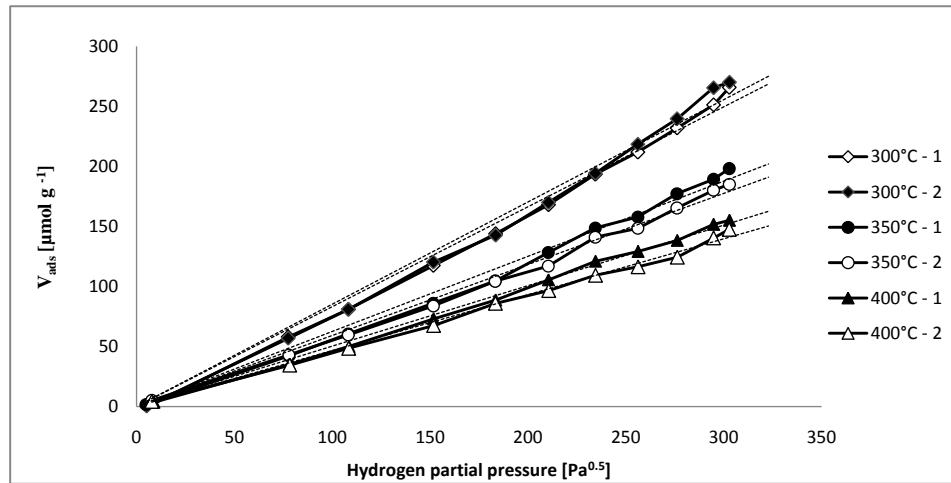


Figure 12: Volumetric adsorption of hydrogen as a function of hydrogen partial pressure for a $4.7\mu\text{m}$ Pd/Ag membrane at 300°C , 350°C and 400°C , with two parallels each. Linear trend lines for each plot are shown as stippled.

Figure 12 shows that solubility decreases with temperature. The linearity of the plot was reduced at higher pressure, and a larger degree of deviation between the two parallels was observed at $>200 \text{ Pa}^{0.5}$. The mean slope of the two parallels were calculated and defined as the solubility constant (K_S). However, only datapoints below $200 \text{ Pa}^{0.5}$ were used, as Sievert's law is invalid at higher pressures, as discussed in section 2.1.1. The Sieverts' constant of $2.2\mu\text{m}$, $4.7\mu\text{m}$ and $10.0\mu\text{m}$ at 300°C , 350°C and 400°C are given in Figure 13.

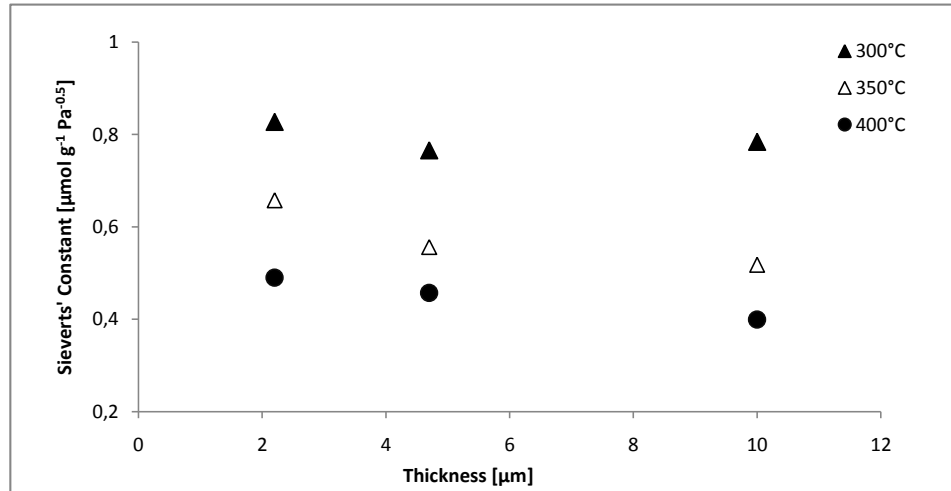


Figure 13: The Sieverts' Constants plotted against the respective membrane thickness at 300°C, 350°C and 400°C

Figure 13 shows an increase in Sieverts' constant with reduced- thickness and temperature, with an exception for 10.0 μm at 300 °C. This datapoint is higher than the respective one for 4.7 μm at 300 °C, and does not follow the overall solubility trend. The hydrogen solubility constant and permeability of the membranes tested were used to calculate the diffusivity by Equation 6. The activation energy was determined by plotting logarithmic hydrogen diffusivity against inverse temperature, and the plot is given in Figure 14. The diffusivity-activation energy relation is described in Equation 5.

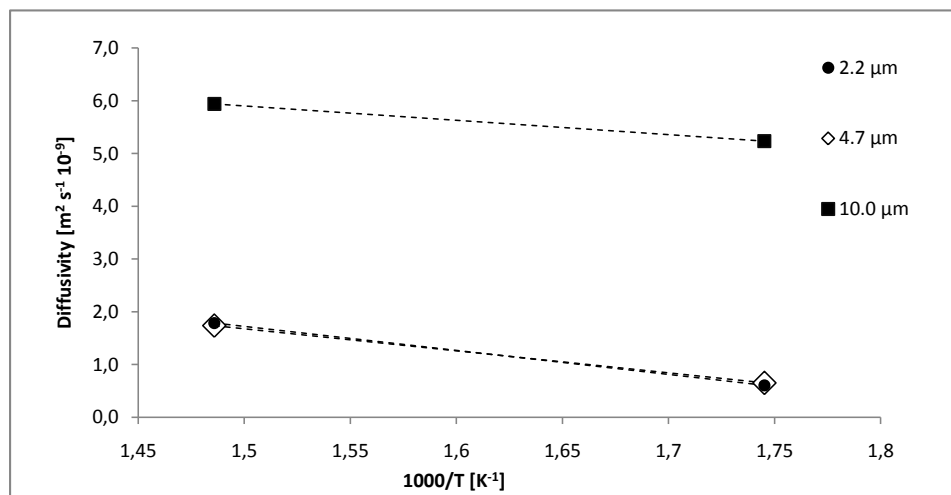


Figure 14: Arrhenius plot of the logarithmic diffusivity versus the inverse temperature for Pd/Ag membranes 2.2 μm, 4.7 μm and 10 μm thick.

Figure 14 displays a steeper slope for $2.2\mu m$ and $4.7\mu m$ membrane compared to $10.0\mu m$. $4.7\mu m$ membranes yields approximately the same diffusivity as $2.2\mu m$ at both $300^\circ C$ and $400^\circ C$. Since there are only two datapoints for each membrane thickness, it yields a perfect fit to a linear line with a coefficient of determination of 1. The activation energies calculated from this plot are given in Table 4 along with comparable values from Vicinanza et al.[52]. The activation energy values showed close similarity to that reported for $10.0/11.2\mu m$. $4.7\mu m$ was determined to be most dissimilar to that reported by Vicinanza. An overall trend showed increasing activation energy with reduced thickness.

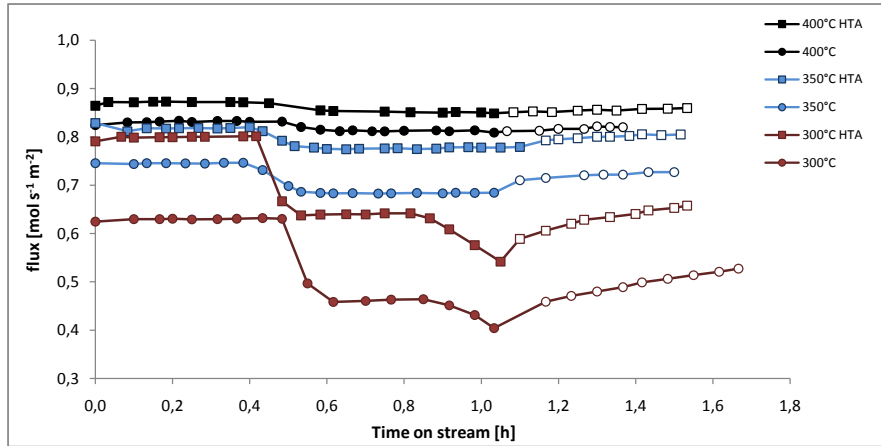
Table 4: Comparison of activation energy for $2.2\mu m$, $4.7\mu m$ and $10.0\mu m$ Pd/Ag membranes in this work, and that of Vicinanz.

Membrane thickness [μm]	Activation Energy [$kJmol^{-1}$]	
	This work	Vicinanza [52]
2.2	35	28
4.7	31	18
10.0	22	-
11.2	-	21

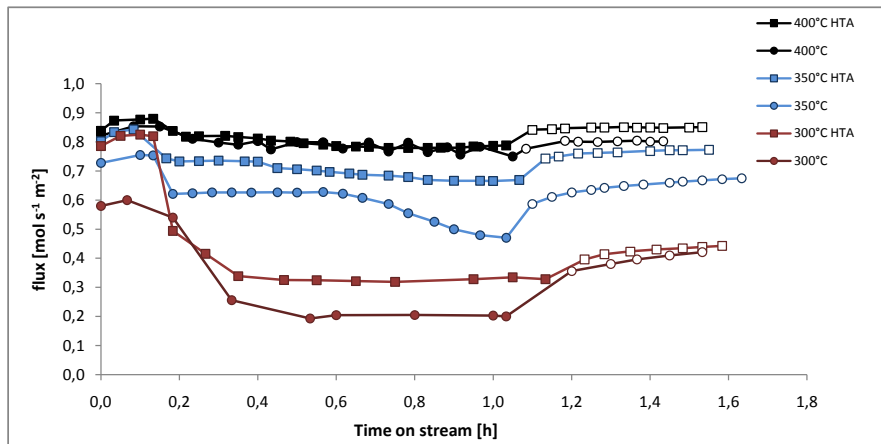
4.2 CO exposure experiments

4.2.1 CO inhibition as a function of temperature, heat treatment in air and CO concentration

The hydrogen flux of a $4.7\mu m$ palladium-silver membrane was monitored with CO exposure over a short period of time. Several CO exposure experiments were performed at different temperatures, CO concentrations and with/without HTA. Figure 15 shows the flux over time at given conditions. The first point at time 0 indicates a stable hydrogen flux, either regenerated or unexposed to CO. The membrane was introduced to CO for one hour, then replaced by N_2 . The flux was monitored for about 90 minutes, with 60 minutes of constant CO concentration (0.5% or 2.0%), and 30 minutes after removal of CO to investigate the regeneration of H_2 flux.



(a)



(b)

Figure 15: Hydrogen flux of a $4.7\mu\text{m}$ Pd/Ag membrane exposed to CO at 300°C , 350°C and 400°C , with and without HTA. Hollow points indicates the regeneration phase where no CO is present. a) 0.5% CO. b) 2.0% CO. Total feed flow consisted of $400\text{NmL}/\text{min}$, $90\%\text{H}_2$, $(10\% - X\%\text{CO})\text{N}_2$

Figure 15 shows a reduction in hydrogen flux for a $4.7\mu\text{m}$ Pd/Ag membrane exposed to CO under different conditions. Reduction in flux was observed to be more severe at lower temperatures, as opposed to high, and heat treated membranes were less affected by the exposure. After one hour, the flux seemed to stabilize at a reduced value relative to the initial flux, for all experiments with the exception of 0.5% CO at 300°C in Figure 15a. Hydrogen flux decreased with increasing CO content in the total feed flow gas. According to Figure 15a the effect of flux reduction was delayed by about 30 minutes at 0.5% CO, whereas an immediate and short lived effect of increased flux was seen in Figure 15b, at 2.0% CO.

4.2.2 Heat treatment effect before and after CO exposure

In addition to investigating a heat treatment in air on membrane before CO exposure, such treatment was done after a sequence of CO exposure experiments(2a-2f) to check regeneration and inhibiting effect of CO. Figure 16 shows the flux over time when exposed to 2% CO at 350°, for a non-HTA membrane, a membrane with HTA before CO exposure and a membrane that underwent HTA after CO. The same experiment was conducted at 400°, and with 0.5% CO at 350° and 400°, associated results are given in Appendix K.

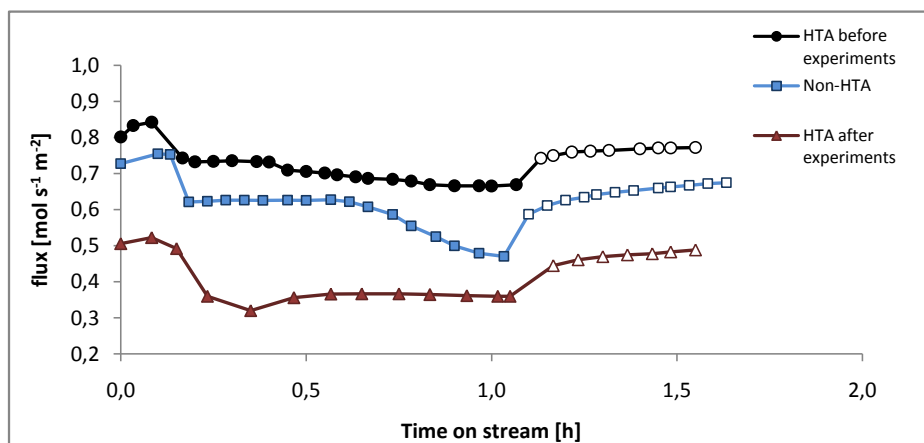


Figure 16: The flux of a 4.7 μm Pd/Ag membrane as a function of time on stream at 2% CO exposure at 350°C, for heat treatment before and after experiment, as well as a membrane only stabilized in hydrogen. Hollow points indicates the regeneration phase where no CO is present.

According to Figure 16 heat treatment before any exposure to CO reduces the inhibiting effect. However, the heat treatment performed after a series of experiment does not show the same improvement in hydrogen flux or resistance to CO exposure. The heat treatment in air after CO exposure was observed to regenerate flux to a higher degree than regeneration in hydrogen permeation, but not back to initial flux. These trends were seen at all temperatures and concentrations, and a membrane that underwent HTA after a series of experiments did not perform better than membrane without heat treatment in air.

4.2.3 Long term exposure of CO on a Pd/Ag membrane

The Pd/Ag membrane of 2.2 μm thickness was exposed to 0.5% CO for ~ 70 hours at 300°C, before CO removal. The regeneration of flux was measured for 47 hours at 300°C, before investigation of flux recovery at 400°C. Figure 17 shows the relative hydrogen flux over time, with and without CO on stream.

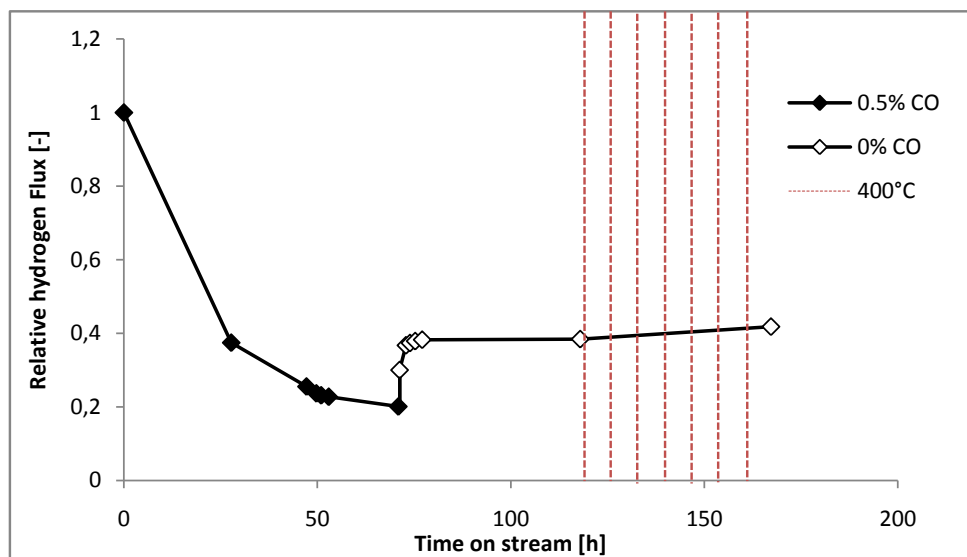
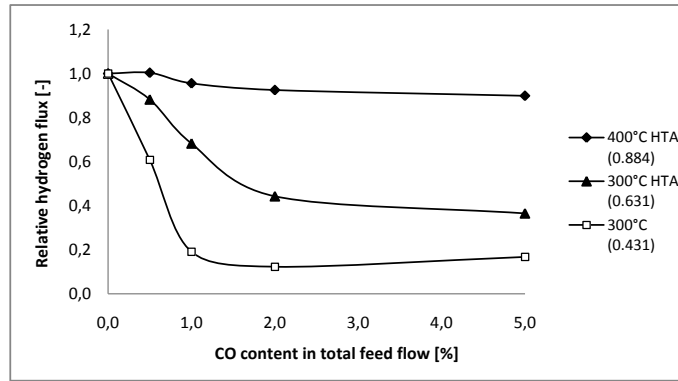


Figure 17: Relative hydrogen flux of a $2.2\mu\text{m}$ Pd/Ag membrane at long-time exposure to 0.5% CO at 300° . Hollow points indicates hydrogen flux after CO removal, and red lines indicates a temperature of 400°C .

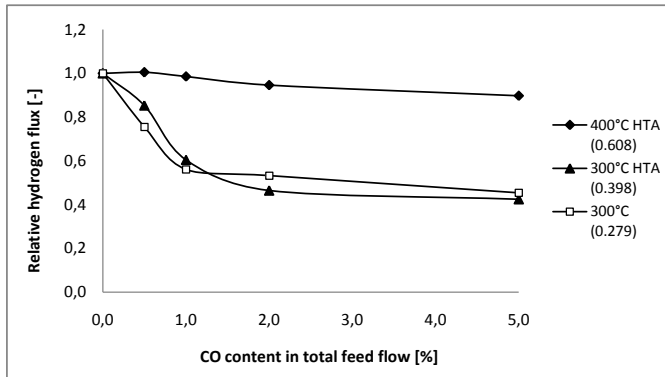
Figure 17 displays a reduction in hydrogen flux of 60% over 20 hours when 0.5% CO is introduced. The hydrogen flux was reduced further over time, and equilibrium was not reached at the time of CO removal, as the flux measurements do not stabilize at one level. Upon removal of CO there was a 17% increase in the flux after two hours. Additional 3% of the flux is recovered after increasing the temperature to 400° , over 50 hours, but the membrane was not regenerated back to initial flux ($1.03\text{ mol s}^{-1}\text{ m}^{-2}$).

4.2.4 CO inhibition effect on different membrane thickness

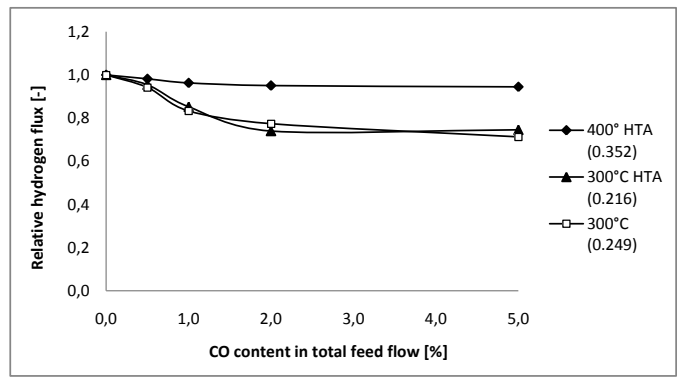
Pd/Ag membranes of $2.2\mu\text{m}$, $4.7\mu\text{m}$ and $10.0\mu\text{m}$ were exposed to CO concentrations of 0-5% at 300°C , and 300°C and 400°C after heat treatment in air. The experiments are labeled 5a-7c, and were conducted with no transmembrane pressure, and Ar as sweep gas on permeate side, as described in section 3.3.6. Figure 18 shows relative hydrogen flux as a function of CO content in the total feed flow.



(a)



(b)



(c)

Figure 18: Relative hydrogen flux at CO exposure concentrations of 0-5%, with no transmembrane pressure difference at 300°C, 300°C HTA and 400°C HTA. a) 2.2 μm , b) 4.7 μm , c) 10.0 μm . Initial flux [$\text{mol s}^{-1} \text{m}^{-2}$] is denoted in parenthesis. Total feed flow of 400NmL/min, 90% H_2 , (10% - X%CO) N_2

As shown in section 4.2.1, Figure 18 illustrates that CO inhibition is dependent on temperature, where high temperature (400°C) have higher hydrogen flux and the CO inhibiting effect is reduced, compared to a lower temperature (300°C). The flux reduction was minimal for all membrane thicknesses at 400°C HTA, however, at 300°C with- and without HTA the flux reduction is dependent on thickness as well. According to Figure 18a the hydrogen flux in presence of CO was strongly dependent on temperature and HTA, whereas Figure 18b and 18c illustrates a decreasing dependency on HTA and temperature. Heat treatment was observed to increase the resistance to CO for a 2.2 μm membrane, but the effect was minimal or not existing in the case of 4.7 μm and 10.0 μm membranes. An increase in CO concentration from 2% to 5% did not yield a significant flux reduction in any of the cases shown above.

4.3 CO and H₂O inhibition effect on different membrane thickness

Hydrogen flux in the presence of both CO and H₂O was investigated on thin (2.2 μm) and thick (10.0 μm) membranes. Both membranes were heat treated before exposure, and was left over night until stabilized flux upon CO and H₂O presence. Flux measurements were taken at 0-4 % CO and H₂O at 300°C, and are shown in Figure 19.

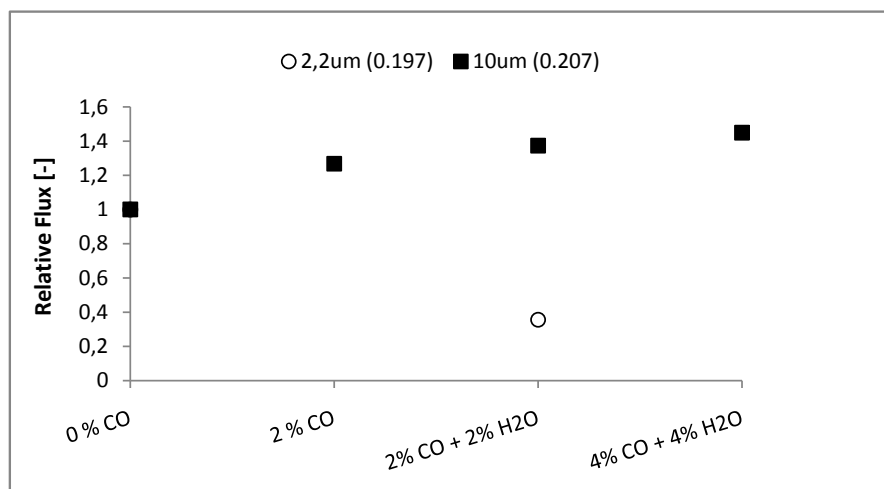


Figure 19: Relative hydrogen flux of 2.2 μm and 10.0 μm Pd/Ag membrane at exposure to 0-4 % CO and 0-4% H₂O at 300°C. Initial flux [$\text{mol s}^{-1} \text{m}^{-2}$] is denoted in parenthesis

Figure 19 provides relative hydrogen flux with CO and H₂O in feed flow. As oppose to previous trends, the hydrogen flux of 10.0 μm Pd/Ag membrane was observed to increase at CO exposure. Further increase in flux was seen as H₂O was added, and with increasing concentration of both components. An examination of the inhibition at 400°C was started, but membrane broke upon the temperature ramping. 2.2 μm Pd/Ag membrane was observed to have a lower initial flux both before and after HTA than 10.0 μm . Different from the thicker membrane, the thickness of 2.2 μm showed a reduction in flux upon 2%- CO and H₂O. This investigation was not completed as the hydrogen flux of 2.2 μm membrane was minimal, and showed extremely poor performance. CO₂ was not detected on micro-GC in retentate flow at any point during runs, as oppose to CO. H₂O presence was validated by water in condenser.

4.4 Deactivation and regeneration of Pd/Ag membrane

Section 4.2.1 showed a reduced hydrogen flux at CO exposure over 60 minutes and regeneration (increase in hydrogen flux) of membrane over an additional 30 minutes. By measuring the regeneration of flux after removal of CO, the deactivation of membrane could be seperated into irreversible and reversible deactivation. The irreversible deactivation was defined to be the percentage of starting flux in experiment that did not recover after 30 minutes in a H₂/N₂ gas mixture. The reversible deactivation was defined as the flux that recovered within the 30minutes after CO removal. Table 5 shows the percentage of deactivation of membrane caused by each short term CO exposure experiment with $\Delta P=1.2$ across the membrane.

Table 5: Deactivation and regeneration of palladium-silver membrane after exposure to CO, for short term CO exposure experiment with total pressure difference across membrane of 1.2 bar. Deactivation is expressed as total flux reduction, and it's irreversible/reversible part, their relationship and total regeneration after a ~ 24 hrs. The irreversible and reversible deactivation are defined by the flux after 30 minutes of regeneration, and adds up to the total reduction.

CO [%]	HTA	T [°C]	Total flux ¹ reduction [%]	Irreversible ¹ [%]	Reversible ¹ [%]	<u>Reversible¹</u> Irreversible ¹	Regeneration ² [%]
0.5	no	400	1.9	1.4	0.5	0.37	99.7
0.5	yes	400	1.8	1.2	0.6	0.45	96.4
2.0	no	400	7.9	5.5	2.4	0.38	99.4
2.0	yes	400	6.0	7.5	-1.5	-0.20	105.6
0.5	no	350	8.2	5.7	2.4	0.42	97.7
0.5	yes	350	6.0	3.1	2.9	0.91	96.7
2.0	no	350	35.4	28.1	7.3	0.26	98.1
2.0	yes	350	16.5	12.9	3.6	0.28	94.1
0.5	no	300	35.3	19.7	15.6	0.79	99.4
0.5	yes	300	31.4	14.6	16.8	1.15	92.7
2.0	no	300	65.5	38.1	27.3	0.72	92.0
2.0	yes	300	58.2	14.5	43.7	3.1	96.0

¹ Defined by hydrogen flux after 30 minutes of regeneration without CO present in feed gas.

² Defined by hydrogen flux ~ 24 hours of regeneration without CO present in feed gas.

According to Table 5 the hydrogen flux reduction of membrane occurred in all experiments. It was observed that deactivation increased with decreased temperature, as previously discussed. The deactivation was more dominant as concentration of CO increased, as expected. Total flux reduction can be separated into irreversible and reversible deactivation, with a varying ratio. Reversible deactivation was mostly dominant at 300°C, while irreversible deactivation was observed to be responsible for most of the inhibition in total. This is shown in the deactivation ratio reversible/irreversible, which was below 1.0 for most experiments. There are trend indications in the deactivation ratio, but significant deviations are observed. The rev./irrev.-ratio is seen to be ~ 0.4 at 400°C, if -0.2 is excluded. The latter value was observed to regenerate to a higher hydrogen flux than initially measured, giving a negative reversible deactivation value, which can be seen in percent regenerated as well (over 100 %). Regeneration of flux after short time CO exposure was observed to be at a minimum of 92% relative to the initial hydrogen flux, before start of experiment. The deactivation was lower for HTA membranes in all cases, with higher significance at more straining conditions. Two membranes were utilized in these experiments; with and without HTA. With slight irreversible deactivation for each experiment adding up, these membranes had an ending flux of 87% and 67% relative to the flux before any experiment or CO exposure, respectively.

4.5 Surface investigation by X-ray photoelectron spectroscopy

The membranes used in permeation experiments were investigated on XPS in order to identify what atom species were chemically bound to the surface. Unused membrane samples of different thicknesses were

investigated on both growth and substrate side, whereas the used membranes were studied only on growth/feed side.

4.5.1 Spectra

XPS spectra of as-grown (unused) Pd/Ag membranes are displayed in Figure 20. Figure 20a shows the growth surface, while Figure 20b shows the surface corresponding to the substrate-film interface during growth.

Figure 20a displays 1s, 3p and 3d peaks for both Pd and Ag, as well as O 1s and C 1s. Valence and Auger peaks are present in the spectra for low and high E_B respectively. Figure 20b shows the same peaks as in Figure 20a with the exception of Si 2s. Silica was not detected in acquisition of substrate $2.2\mu\text{m}$ and $10\mu\text{m}$ membrane, or any growth samples. The silver peaks, such as Ag 3d $5/2$, are significantly higher on substrate side than growth side, and palladium peaks such as Pd 3p $1/2$ are lower. This is looked further into in the quantitative analysis in section 4.5.2.

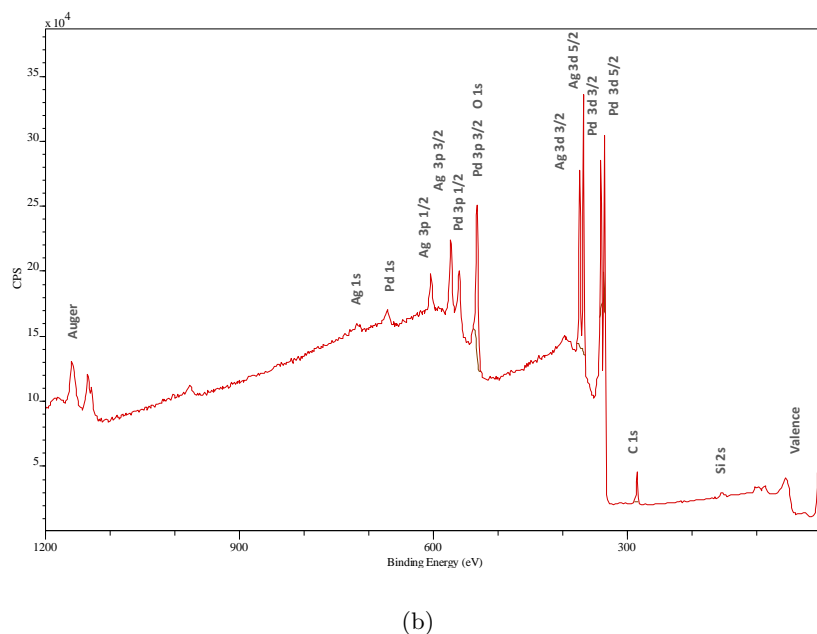
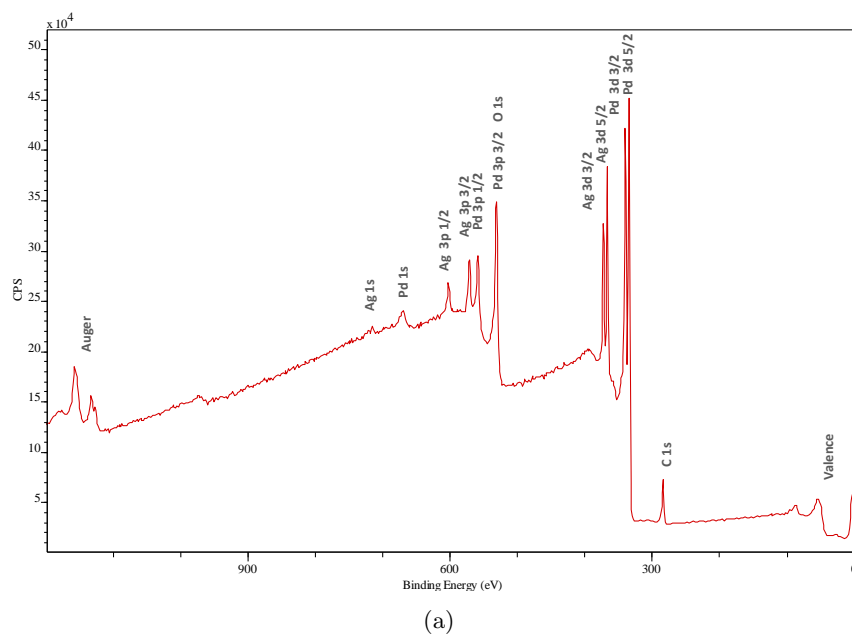
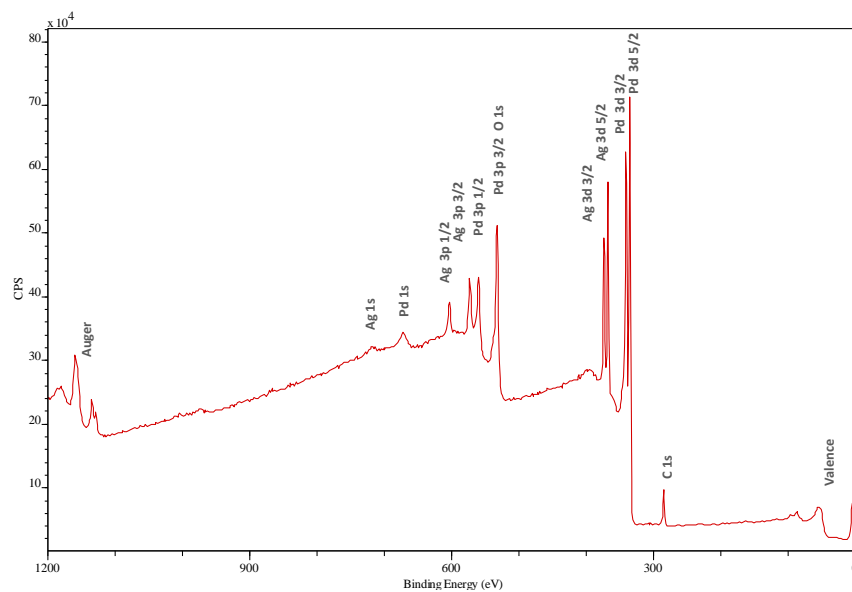


Figure 20: XPS Survey spectrum of a) unused growth side $4.7\mu\text{m}$ Pd/Ag membrane, b) unused substrate side $4.7\mu\text{m}$ Pd/Ag membrane.

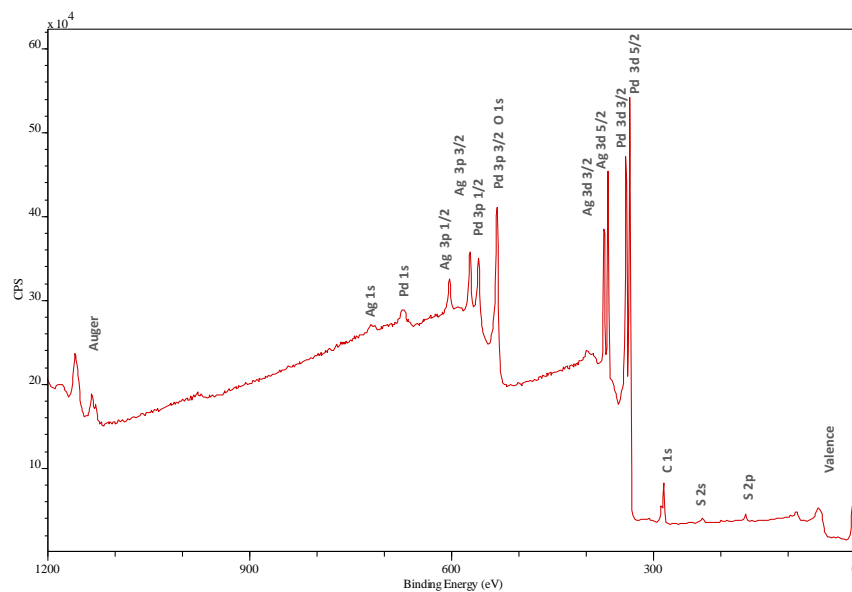
The growth/feed surface of two other $4.7\mu\text{m}$ Pd/Ag membrane samples previously utilized in experiments were investigated with XPS. Figure 21a shows a XPS spectrum of the membrane used in experiment 4a

through 4f, meaning there was HTA performed on the membrane before any CO exposure experiments were conducted. The survey spectrum given in Figure 21 displays a growth/feed surface of a 4.7 μm Pd/Ag membrane previously used in experiment 2a through 3d. The membrane was exposed to CO in six sequential experiments before it underwent HTA, and was further utilized in four additional experiments exposing it to CO.

Both spectra in figure 21 shows similar peaks and binding energies to that of an unused growth side membrane in Figure 20. However, Figure 21b shows a spectrum of a Pd/Ag surface contaminated with traces of sulphur, as indicated by S 2s and S 2p peaks. No sulphur poisoning were detected on any other samples investigated on XPS. In comparison, Figure 21a has no additional peaks detected relative to the unused growth spectrum. The XPS survey spectra of 2.2 μm and 10.0 μm are given in Appendix L.



(a)



(b)

Figure 21: XPS Survey spectrum of a) growth/feed side $4.7\mu\text{m}$ Pd/Ag membrane that underwent HTA before CO exposure, b) growth/feed side $4.7\mu\text{m}$ Pd/Ag membrane that underwent HTA after CO exposure, then subjected to further CO exposure.

Figure 22 compares the different carbon 1s peaks from three different Pd/Ag surfaces. The top peak is the $4.7\mu\text{m}$ membrane unexposed to any experiment (Figure 20a), whereas the two other were investigated after

experiments. Middle spectrum underwent HTA before any experiment was conducted (Figure 21a), and bottom spectrum underwent HTA after a series of experiment involving CO (Figure 21b).

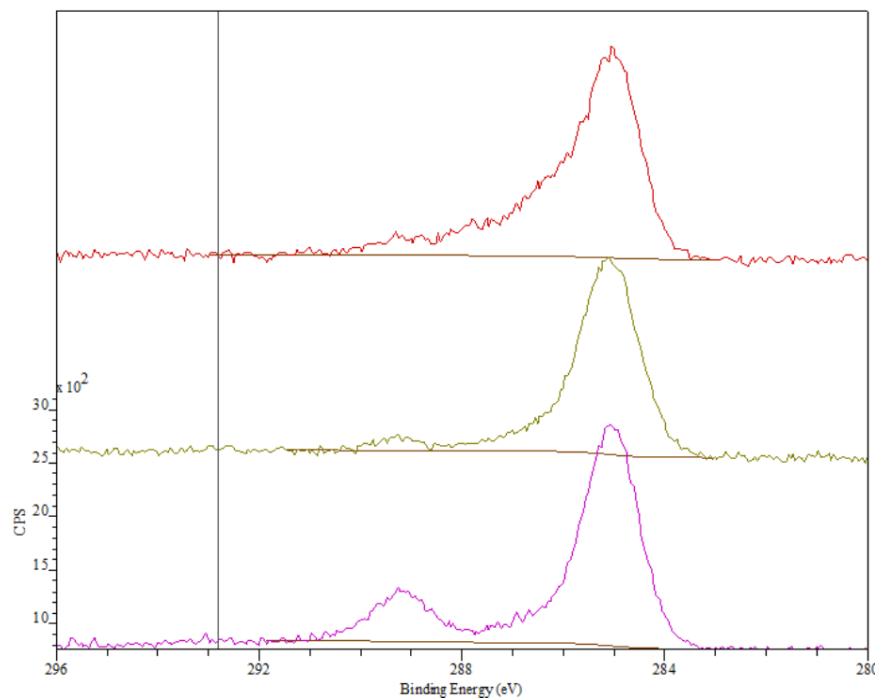


Figure 22: Overlaid and normalized C 1s peak spectrums. **Top**) As-Grown $4.7\mu\text{m}$ Pd/Ag membrane. **Middle**) Growth/Feed $4.7\mu\text{m}$ Pd/Ag membrane from experiment 4a-4f. **Bottom**) Growth/Feed $4.7\mu\text{m}$ Pd/Ag membrane from experiment 2a-3d.

According to Figure 22 there is a difference in carbon species on the membrane surfaces, dependent on their use. The spectrum indicates that there is more than one carbon peak, with the asymmetric tail and the additional peak on the high energy side. This is further shown in the fitting of the curves in section 2.4.2, where three or four components are used per fitting of carbon spectrum. The membrane surface that underwent HTA before use is observed to have least carbon species on the surface, while the membrane with CO exposure before and after HTA is shown to have most, by the total lineshape area. The latter is seen to have a significant peak growth at a binding energy of ~ 289 eV. The asymmetric tail of the unused membrane is observed to have a different shape than the ones utilized in experiments.

4.5.2 Quantification

The membranes utilized in this project were investigated by XPS, and the components present on the membrane surfaces were quantified by calculating the area of fitted synthetic line shapes. Only Pd 3d $5/2$ Ag 3d $5/2$ were used in the quantification done, to reduce the errors from sensitivity factors. Table 6 shows relative amounts of Pd, Ag and C on the membranes thicknesses $2.2\mu\text{m}$, $4.7\mu\text{m}$ and $10\mu\text{m}$ both Substrate and As-Grown sides, with two additional used $4.7\mu\text{m}$ membranes.

Table 6: Relative amount of species on Pd/Ag membranes investigated by XPS spectra

Membrane thickness [μm]	Side	$\frac{Pd}{Pd + Ag}$ [%]	$\frac{Ag}{Pd + Ag}$ [%]	$\frac{C}{Pd + Ag}$ [%]	Experimental exposure
~ 2.2	Growth	69	31	4	No experiment
~ 2.2	Substrate	62	38	6	No experiment
~ 4.7	Growth	69	31	9	No experiment
~ 4.7	Substrate	60	40	7	No experiment
~ 10	Growth	69	31	7	No experiment
~ 10	Substrate	62	38	6	No experiment
~ 4.7	Growth/Feed	66	34	10	CO - HTA - CO - H ₂
~ 4.7	Growth/Feed	67	33	6	HTA - CO

Table 6 indicates a silver enrichment relative to the growth side on all substrate side samples. Despite not being exposed to CO experimentally, both substrate and growth samples contained carbon species. The membranes exposed to CO experimentally did not show a significantly higher amount of carbon than the unused ones in comparison, and no clear trends were observed on the carbon quantification. Growth/feed side membrane with the most severe experimental exposure and treatment did have the highest relative amount of C on the surface, followed closely by a unused growth sample of $4.7\mu\text{m}$ thickness. It should be noted that the growth/feed with most C present was regenerated with pure H₂ permeation, whereas the growth/feed with the least amount of C on surface was not regenerated, but taken straight from CO exposure to inerts, then XPS investigation. No standard/reference was used on the surface to accurately quantify the amounts of species, but the overall peak ratio is approximately 70/30 Pd/Ag.

5 Discussion

5.1 Pd/Ag membrane properties

The permeability and permeance of membranes used in this work were observed to be in the same range, but generally lower than what is reported by Mejdell et al. and Vicinanz et al. [28, 52] for Pd/Ag membranes provided by SINTEF Materials and Chemistry in Oslo. Experiments performed with a transmembrane pressure difference of 1.2 bar showed higher permeability than reported. This difference may be due to high pressure differences causing metal stretching, increasing membrane permeation area [28]. Mejdell and Vicinanz's [28, 52] had generally higher values, but specified using feed pressures when measuring flux. It is evident that higher transmembrane pressure differences are applied, permeability values increase. Hence sweep gas as a driving force does not get as high permeability values as feed pressure do, but will keep from material stretching. The partial pressure of hydrogen gas may be different at membrane surface than calculated from bubbleflow meter and Micro-GC, especially if concentration polarization occurs. In this case the values of permeability and permeance will be inaccurate, and possibly lower than expected. Correct sweep gas flow is therefore important in order to reduce concentration gradients at membrane surface. Permeability is in principle a material constant if the bulk diffusion is the transport limiting step for membranes of same composition, thickness and structure. Variations in permeability values in this work can also be due to thickness variations over a single Pd/Ag covered wafer, different storage times or contaminations. It was shown that all permeance values for 10.0 μm membranes were close to that of bulk limitations reported [3]. It is evident that thinner membranes ($\leq 5 \mu\text{m}$) are limited by surface phenomena, as the permeability deviates from that reported for a bulk limited membrane at 300°C. Clearly, membranes in this work are in agreement to what is reported by Mejdell and Vicinanz. They state that bulk diffusion is limiting for thicker membranes ($\geq 5 \mu\text{m}$), whereas thinner ones are limited by surface effects at 300°C [4, 5]. The 4.7 μm Pd/Ag membrane is in this work observed to not be bulk-limited at 300°, with $\Delta P = 0$, which is consistent with literature. However, 4.7 μm does not show complete surface limitations, indicating it is a compromise between the two limitations. Permeability values at 400° have different temperature dependencies than at 300°, thus not compared.

Hydrogen permeation was observed to increase in the temperature range of 300-400°C, for all the experiments done. This is in agreement of what has been reported previously [54, 55]. This could possibly be explained by increased transport of atomic hydrogen through membrane bulk with temperature. Which means both bulk- and surface limited membranes have increased permeation with temperature. In the case of a thin membrane, surface effects are most likely the limiting step of the transport. The hydrogen adsorption is dependent on temperature through Arrhenius equation (Eq.13) and Langmuir isotherm. This dependency shows that lower temperatures will give stronger bonds between the atomic hydrogen and the palladium-silver surface, thus permeation of thin membranes are increased with temperature on both surface and through bulk. Permeability is dependent on both the solubility constant and diffusivity, which are both dependent on temperature, as shown in section 2.1.1. There is a trade-off with increased temperature as solubility decreases and the diffusivity increases. In the case of Pd/Ag23.wt%, permeability was observed to increase with temperature, meaning diffusivity increases more than solubility decreases. However, this may be due to the H₂ adsorption model as a function of temperature.

Heat treatment in air was observed to increase the permeability of the Pd/Ag membranes, in compliance with other works [28–34, 37]. The treatment procedure has a reduced effect on thicker membranes as oppose to thinner ones, as reported in literature [28, 37] which states that permeability approaches a constant value of $2.1 \cdot 10^{-8} \text{ mol m s}^{-1} \text{ m}^{-2} \text{ Pa}^{0.5}$ at 300°C . The mean permeability value at 300°C for heat treated membranes here is comparable, with a value of $1.9 \cdot 10^{-8} \text{ mol m s}^{-1} \text{ m}^{-2} \text{ Pa}^{0.5}$. Peters et al. found the n -value to decrease upon HTA, which indicates that transport limitations of the Pd/Ag membrane is moved from surface to bulk [36].

Volumetric sorption technique was used to determine the solubility constant of some membranes utilized. The solubility constant decreases with temperature for all thicknesses, as described in Equation 7. There was some degree of deviation between the two subsequent measurements at high pressures, which indicates that sorption- or experimental effects are contributing. Irreversible adsorption could possibly be a factor, reducing sorption area, giving variation in the two measurements. Linear fittings of the isotherms were however based on data points below $200 \text{ Pa}^{0.5}$ which defines the valid region of Sieverts' law. The amount of measurements taken in this region could be expanded in order increase accuracy and validity.

The solubility constant was found to be dependent on thickness, which could be unexpected, as the solubility constant is an intrinsic material property, and should be independent of material form. This was however discovered by Vicinanza and coworkers as well [52]. The solubility was observed to decrease with increased membrane thickness, with one inconsistent data point for $10.0 \mu\text{m}$ at 300°C . Vicinanza et al. concluded by atomic force microscopy (AFM) that the trend of decreasing solubility with increasing membrane thickness is due to lower average density of grain boundaries for thicker Pd/Ag films, where surface roughness on growth side increases with membrane thickness [52]. The increase of surface roughness with membrane thickness for Pd/Ag membranes provided by SINTEF has previously been reported by use of AFM [28, 33] as well as X-ray diffraction (XRD) and transmission electron microscopy (TEM) [34].

The membrane diffusivity was calculated through permeability- and solubility values acquired experimentally, and membrane activation energy was obtained by plotting the diffusivity against inverse temperature. Activation energies were extracted from trendlines based only on two measurements which gives a perfect linear fit. In retrospect, more datapoints should have been measured and used. The activation energies of $2.2 \mu\text{m}$, $4.7 \mu\text{m}$ and $10.0 \mu\text{m}$ Pd/Ag membranes were compared to respective thicknesses from Vicinanza and coworkers' work [52], and showed close similarity. A membrane of $10.0 \mu\text{m}$ was calculated to have an activation energy of 22 kJ mol^{-1} while Vicinanza reported 21 kJ mol^{-1} for a thickness of $11.2 \mu\text{m}$. Both values are close to that reported by Holleck [16], of 22 kJ mol^{-1} (5335 cal g^{-1}) for a $\text{Pd}_{80}\text{Ag}_{20}$ with a thickness range of 0.0800 to 0.2025 cm . With the assumption that a transport through a Pd/Ag membrane of 0.0800 to 0.2025 cm thickness is only bulk limited, activation energy will be $\sim 20\text{-}22 \text{ kJ mol}^{-1}$, which indicates bulk transport limitations for a $10.0 \mu\text{m}$ Pd/Ag membrane as well.

The activation energy of a $2.2 \mu\text{m}$ Pd/Ag membrane was calculated to have an activation energy of 35 kJ mol^{-1} , corresponding well to 28 kJ mol^{-1} stated by Vicinanza [52]. The higher activation energy observed is dissimilar to the bulk limited membranes where $E_a = \sim 20\text{-}22 \text{ kJ mol}^{-1}$. Thus, transport limitations in thinner membranes with higher activation energies are assumed to be governed by surface processes. $4.7 \mu\text{m}$ can possibly be controlled by both surface and bulk limitations, but surface phenomena is assumed the most dominant as $E_a = 31 \text{ kJ mol}^{-1}$. When surface phenomena is the rate limiting step, the assumption

of proportionality between hydrogen flux and the square root of partial pressure no longer holds, hence n -value \neq 0.5. When the rate limiting step of transport is only limited by surface processes, the n -value=1. By varying n -value, the best linear fit between hydrogen flux and hydrogen partial pressure difference can be obtained. Peters et al. found $n=0.79$ for 1.9-3.8 μ m non-HTA membrane [36], while Mejdell et al. found $n=0.61$ for a 1.4 μ m membrane [56]. This indicates that thinner membranes most likely are not governed only by surface processes, but have some bulk limitations as well. Vicinanza et al. [52] claims no significant change in E_a as 1 and 0.7 are applied as n -values for calculational purposes. The value of n is not investigated thoroughly in this work, and all calculations have used a value of 0.5. To further validate assumptions made, hydrogen flux plotted against $P_{ret}^n - P_{perm}^n$ could be done with varying n for best linear fit. Determination of exact n -values have proven to be difficult as very wide pressure ranges are required [36, 56]. Permeability value is affected by other parameters as well, such as composition gradients, material structure, fabrication method, concentration gradients, set-up conditions and measurements. The adsorption of hydrogen onto palladium surfaces have been reported to be almost without barriers [39]. However, desorption is stated to have a larger barrier, which is increased with the presence of silver [57]. Hydrogen desorption at membrane substrate side may be the transport limiting process in thin membranes, and the silver enrichment on the Pd/Ag membrane substrate side found by XPS further validates this assumption.

5.2 The inhibiting effect of CO on Pd/Ag membrane

The site coverage of CO on the surface is determined by pressure and temperature, as stated in the Langmuir expression and Arrhenius Equation 14 and 13, in section 2.1.3. This was shown experimentally as the inhibiting effect of CO on palladium surface was investigated. Hydrogen permeation was observed to decrease with increased CO concentrations, in compliance with literature which states that inhibition of the palladium surface increases with partial pressures of CO [22, 54, 55]. Short term CO exposure experiments showed that with 2.0% CO in total feed, the hydrogen flux had an immediate increase for all experiments before inhibition occurred. There was no instant drop in hydrogen permeation at 0.5 % CO exposure, and it generally took some time before the inhibition of surface sites occurred and flux was reduced. With high gas velocity (400NmL/min) in the set-up this could possibly be considered a surface effect. There was no significant delay of CO from source to membrane when detected by Micro-GC. None of these unexpected effects are similar to any reported cases found, neither the immediate flux increase in flux at 2% CO introduction, or the 30 min delay at 0.5% CO.

Increased temperatures displayed a reduced inhibiting effect of CO, in agreement with reported observations [40, 41, 54, 55]. It is apparent that CO adsorbs competitively on the palladium surface with hydrogen. This is indicated by the significant reduction in hydrogen flux upon CO introduction. Thus, surface adsorption is considered the main rate determining step of permeation when inhibited by CO. 10.0 μ m Pd/Ag exposed to 0-5% CO at 400°C shows little to no deactivation, possibly being limited by bulk diffusion only. It is noticeable how the membranes can be limited by both effects. The competitive adsorption of H₂ is favored at high temperatures in a system with CO according to the observations made. This is due two different temperature dependencies of CO and H₂, as shown in the Langmuir expression.

The deactivation of a 4.7 μ m palladium-silver membrane was determined not to regenerate back to its initial stage at any point, with a few instances where regeneration was close to complete, e.g. 99.7% (0.5% CO at

400°C). This means that some site deactivation is irreversible, or the right method of regeneration is not utilized. The membranes were seen to recover over time with hydrogen on stream, in agreement with Li et al. [55]. Most deactivation at CO exposure is irreversible, and generally the ratio Reversible/Irreversible-deactivation increases with CO concentrations and lower temperatures. Desorption of CO may be hindered at lower temperatures due to energy barriers. The lowest ratio of reversible/irreversible deactivation is observed with 2.0 % CO at 350° CO, deviating from the overall trend. Li et al. [55] reports CO adsorption to be the predominant deactivation mechanism at temperatures below 350°, while carbon deposition occurs at higher temperatures. Similarly permanent deactivation can be considered to be the irreversible adsorption of CO, as temperatures never exceed 400°. Coke formation on the metal surface may occur, but catalytic activity on Pd metal membrane is reported to take place with CO concentrations of 20-30% of feed flow at higher temperatures than utilized in this work [55]. Irreversible adsorption may in fact be reversible at other temperatures, and deactivation can possibly be effected by other phenomena as well. After being utilized in several experiments with only partial regeneration in between, the 4.7 μ m membranes with- and without heat treatment in air had a final flux of 87- and 67% relative to initial flux. This shows that heat treatment in air procedure increases resistance to CO and valuable lifetime is possibly gained.

Membranes exposed to CO were never fully regenerated back to their initial flux. This means that the starting flux presented in figures have already been effected by CO, and in most cases been inhibited irreversibly. Consequently the data are not as comparable as possible, since membranes were used in several experiments. This was done due to the fact that Pd/Ag material is highly expensive, and the installation of new membrane for each experiment would be time inefficient. The order of experiments was planned to decrease high amount of deactivation early, and to keep permeability high for as long as possible. This was done by doing elevated temperatures and low CO content early, and more straining conditions later. Mejdell et al. suggests that regeneration of hydrogen flux after CO is more difficult at higher pressures [56]. Regeneration and deactivation is in this work only investigated with experiments at 2.2 bar on feed side. Examination and comparisons of CO inhibition with total feed pressure and sweep gas only should be done.

The inhibiting effect of CO on the membrane was observed to be lower for a membrane that underwent HTA, which is in compliance to what Mejdell et al. reported [35]. It is reported that a heat treatment in air increases the surface area through roughening [28, 33, 52], which may increase adsorption and desorption sites for hydrogen. Meaning, if membrane transport of hydrogen is limited by surface processes, the permeability increases after HTA. Site alteration may favor H₂ adsorption over CO, reducing the inhibiting effect. Mejdell et al. [35] uses a modelling study combining model equation from Barbieri et al.[58] and microkinetic modeling to indicate that a restructuring due to oxidation-reduction changes heats of adsorption, but are unable to predict the effect on the competitive adsorption of H₂ or CO. However, with a reduced inhibiting effect of CO after HTA, H₂ adsorption can be assumed to be favored on surface. HTA was performed before and after membrane was exposed to CO, and indicated significant differences. By heat treating after several exposure experiments the hydrogen flux was lower than for untreated membrane and was more affected by further CO introduction. There is a great difference in performance dependent on whether HTA is performed before or after CO exposure. It is evident that Heat treatment in air has a positive effect when applied before CO exposure.

Regeneration of membrane was observed for both HTA after and before, showing that the treatment can

remove impurities, in agreement to literature [40, 41]. The oxide layer formed after HTA [27] could possibly interact with CO, forming CO₂, which will cause a reduced inhibition of Pd-surface. However, the oxidelayer was subsequently reduced with H₂ present, and no CO₂ was detected on retentate side by micro-GC. In the case of CO₂ presence, it is below the detection limit of equipment and calibrations.

After 50 hours of exposure to 0.5 % CO at 300°C the flux of a 2.2 μ m Pd/Ag 23 wt.% membrane was reduced by 60% . After CO removal the membrane only regenerated 20 % of initial flux over 90 hours, even with an increase in temperature to 400°C for 50 hours. In comparison a 4.7 μ m Pd/Ag 23 wt.% membrane exposed to 0.5 % CO at 300°C for an hour had a reduction in flux by 30%, followed by a recovery of 20 % over an hour without CO. The two results are difficult to compare specifically as there may be a thickness dependencies. The results are however interesting, as time of CO exposure may be a key factor to membrane inhibition and regeneration, and longer exposure may cause a higher fraction of irreversible/reversible adsorption of CO on Pd/Ag surface. Long term CO exposure experiments should be done on thicker membranes to compare the effects.

0-5% CO exposure was investigated with membrane thickness of 2.2 μ m, 4.7 μ m and 10.0 μ m with no transmembrane pressure difference. Heat treatment was observed to reduce the inhibiting effect for 2.2 μ m, but had smaller effect for 4.7 μ m and 10.0 μ m, with the latter to be least affected. Vicinanza et al. showed that the beneficial effects of HTA occurred in thinner ($\geq 5\mu$ m) membranes, as surface restructuring is one of the main attributes to HTA [37]. Temperature dependency of the hydrogen flux with CO on stream was observed to increase with reduced thickness. 2.2 μ m membrane was mostly effected by temperature as transport is limited by adsorption/desorption, which is a function of temperature. As discussed earlier, the 10 μ m membrane is limited by bulk diffusion, meaning heat treatment and temperature will not effect transport to the same degree as 2.2 μ m. As mentioned earlier in this chapter, the permeability of a bulk limited membrane can increase with temperature as diffusivity increases, explaining the high flux at 400°C relative to 300°C for a thicker membrane. 4.7 μ m thick membranes were assumed to be governed by both surface effects and bulk diffusion, as it displays properties similar to both 2.2 μ m and 10.0 μ m. The hydrogen flux was observed to vary between the CO range of 0-2%, while the reduced flux stabilized at 2-5%.

Hydrogen flux was monitored for 2.2 μ m and 10.0 μ m Pd/Ag membranes in the presence of CO and H₂O. Unexpectedly, an increase in hydrogen flux of 10.0 μ m membrane was observed at exposure to CO and H₂O. Arstad et al. states that CO inhibits a thin membrane, and H₂O contributes with only a dilutional effect [3]. Earlier results and reports indicate that thicker membranes are bulk limited, therefore components affecting surface processes should have restricted effect on 10.0 μ m Pd/Ag membranes. This membrane was however utilized in earlier experiments involving CO exposure, and was left in ambient conditions over several weeks. It is also notable how the membrane broke upon further temperature ramping. The increase in hydrogen flux may have been a result of an already broken membrane, leaking undesired components into permeate flow. This could not be verified as permeate flow was not condensed, and a concern of H₂O in Micro-GC was raised. The Pd/Ag membrane of 2.2 μ m thickness showed extremely poor permeation properties, with hydrogen flux lower than for 10.0 μ m. Heat treatment in air did improve the performance shortly, before stablization at 0.197.mol s⁻¹ m⁻². During exposure to CO and H₂O the flux was reduced to a value close to zero, consequently experiment was cancelled. This membrane was of the same batch as other 2.2 μ m membranes previously investigated. A possible reason for the poor performance may be due to faults in

production, experimental set-up, procedure or contamination of surface. No CO₂ was detected in retentate stream during experiments, which indicates conditions not favoring water gas shift activity on palladium.

5.3 Surface investigation by X-ray photoelectron spectroscopy

In this work the surface of a Pd/Ag membrane was investigated by XPS, and the signature peaks were identified by appropriate software. The binding energy of palladium bulk 3d 5/2 was measured to be ~ 335.3 eV, and are comparable to that of an oxidized Pd₇₅Ag₂₅ surface, found by Walle et al.[59] to be 335.4 eV. Ag 3d 5/2 was found to be ~ 367.8 eV. The quantified peak ratio of $\sim 70/30$ on growth side agrees reasonably well with the membrane composition of 77/23wt.% Pd/Ag. The Pd/Ag distribution was determined to have a silver enrichment shift on substrate side relative to the growth-side, for all as-grown (unused) samples. This may be due to the patented two-step magnetron sputtering process [51] in which the Pd/Ag membranes are made. Svenum et al. based on theoretical electronic ground state predictions state a strong segregation of Palladium to surface under heat treatment in air as the surface is oxidized [38], and similar effect could possibly argument for the Pd-enrichment on as-grown membrane side exposed to air. Heat treatment in air however, is done at elevated temperatures, and may not hold for this case where oxidation occurs at room temperature where atoms are less likely to migrate. The detection of Si 2s peak in one of three substrate spectrums can be assumed to originate from the silicon wafer on which the membrane is sputtered, or contaminated equipment.

Oxygen and carbon species were present on all surface samples investigated, without any clear trends on their respective amounts. Literature states that these surface components detected by XPS originates from air exposure and excludes irreversible build-up of oxygen and carbon in a used membrane [3, 33]. Carbon species of used membranes did not significantly surpass unused ones in amounts, but did have a different shape with an additional peak rising on the high energy side. The membrane that underwent HTA before experimental exposure to CO showed less carbon components in comparison to the others. This is in agreement with Yang et al. who report a decrease in surface carbon concentration from 67 to 32% after HTA [60]. The membrane utilized with HTA after a series of experiments contained sulphur. HTA can therefore be suggested to reduce carbon species on surface when applied before CO exposure at elevated temperatures, and may hinder sulphur poisoning of the Pd/Ag surface. Associated, Yang et al. claims a cleaning of surface where sulphur impurities are oxidized to sulfate species [60]. The source of sulphur may originate from the experimental set-up, gas lines or contaminations. No sulphur was detected by micro-GC on retentate or permeate side during experiments. The palladium contributions were found to vary by a high degree, for the used membranes. These results are only shown in Appendix I, Figure A10 and A11. Many factors can possibly be affecting these measurements, as the membrane have undergone heat treatment, CO exposure experiment and ambient air exposure. Thus it is difficult to draw conclusions, and further studies should be done with separate treatments.

Only two membranes utilized in the experimental set-up were investigated, and more data should be recorded before any clear conclusions can be made. Comparisons should have been done with a HTA without any further experiments as well. Quantifications made may contain errors due to different intensities of spectrum and sensitivity factors, and the amount of signature peaks examined can be increased. The amount of samples studied should be increased for the purpose of accuracy, and the curve fittings may contain errors as there are

few pure element peaks, but broad contributions from several components. Further studies should consider an acquisition etching process to conclude bulk and surface contributions in the spectrum, since top bulk provides signals on XPS as well.

6 Conclusion and further work

Hydrogen permeability through Pd/Ag 23wt.% of thickness $2.2\mu\text{m}$, $4.7\mu\text{m}$ and $10,0\mu\text{m}$ membranes increased over a temperature range of 300°C - 400°C . Transport through thinner membranes ($2.2\mu\text{m}$) is limited by surface adsorption and desorption. Heat treatment restructures the Pd/Ag surface, and this seems to result in increased hydrogen permeation for thin membranes. Membranes heat treated in air show very similar permeability, and are assumed to become bulk limited by the treatment. Therefore no or little enhancement is seen in permeability of thicker membranes ($10\mu\text{m}$) after HTA, because transport is already governed by bulk diffusion. $4.7\mu\text{m}$ shows a compromise of the two limitations dependent on conditions. Solubility decreases with temperature and increased membrane thickness, while diffusivity increases. The activation energy was found to increase with decreasing membrane thickness, reflecting a change in the limiting phenomena.

CO inhibition on the membrane surface reduced the hydrogen flux through the Pd/Ag membrane and the reduction of flux increased with CO concentration/partial pressure, clearly indicating that adsorption to surface is the rate determining step. With no significant reduction in flux with CO present, the membrane transport can be assumed to be bulk limited. Heat treatment in air procedure and high temperatures reduced the CO inhibition effect, confirming previous findings for similar membranes. There was reversible adsorption of CO on the palladium-silver surfaces in nearly all cases, but irreversible deactivation was the most dominant deactivation in short term experiments. Long term exposure to CO may cause severe reduction in hydrogen permeability and a higher degree of irreversible adsorption than short term.

The unused Pd/Ag membranes were determined to have a silver enrichment on substrate side by performing surface investigations with XPS. Carbon and oxygen species were found in all samples, and can be assumed to result from exposure to air. Membranes exposed to CO displays different C 1s peak positions, dependent on exposure time and heat treatment, where a membrane heat treated in air showed slightly less carbon. Due to the masking of C-signal because of sample transfer under air, no definite conclusion on carbon build-up can be made.

Better regenerational procedures could be investigated in order to lengthen the lifetime of the palladium-silver membrane. Long term exposure to CO should be further studied to check possible industrial performance, as well as the effect of CO_2 , CH_4 and H_2O in feed flow. Additional characterization of the palladium membrane should be done before and after the exposure to the CO, to determine what deactivation mechanisms is present, such as XPS *in situ* and IR spectroscopy. XPS should also be performed with an depth profiling to determine bulk and surface contributions in spectra, as well as further quantifications with more peaks included. A cost analysis can be performed estimating: lifetime, production cost, thickness versus permeability investigations and more material strength/brittleness.

7 References

- [1] J.A. Moulijn, M. Makkee, and A. Van Diepen. *Chemical Process Technology*. John Wiley & Sons Ltd, Chichester, 2001.
- [2] E.D Park, D. Lee, and H.C. Lee. Recent progress in selective CO removal in a H₂-rich stream. *Catalysis Today*, 139(4):280 – 290, 2009.
- [3] B. Arstad, H. Venvik, H. Klette, J.C. Walmsley, W.M. Tucho, R. Holmestad, A. Holmen, and R. Bre-desen. Studies of self-supported 1.6m Pd/23wt.% Ag membranes during and after hydrogen production in a catalytic membrane reactor. *Catalysis Today*, 118(12):63 – 72, 2006.
- [4] A.L. Mejdell. *Properties and application of a 1-5 um Pd/Ag23wt.% membranes for hydrogen seperation*. PhD thesis, Norwegian University of Science and Technology, 2009.
- [5] N. Vicinanza. *An investigation of fundemental phenomena affecting the performance of sputtered Pd-Alloy thin film membranes for hydrogen seperation*. PhD thesis, Norwegian University of Science and Technology, 2014.
- [6] R. Hughes. Composite palladium membranes for catalytic membrane reactors. *Membrane Technology*, 2001(131):9 – 13, 2001.
- [7] T.L. Ward and T. Dao. Model of hydrogen permeation behavior in palladium membranes. *Journal of Membrane Science*, 153(2):211 – 231, 1999.
- [8] A.L. Athayde, R.W. Baker, and P. Nguyen. Metal composite membranes for hydrogen separation. *Journal of Membrane Science*, 94(1):299 – 311, 1994.
- [9] J.T.F. Keurentjes, F.C. Gielens, H.D. Tong, C.J.M. van Rijn, and M.A.G. Vorstman. High-Flux Palladium Membranes Based on Microsystem Technology. *Industrial & Engineering Chemistry Research*, 43(16):4768–4772, 2004.
- [10] J.P. Collins and J.D. Way. Preparation and characterization of a composite palladium-ceramic membrane. *Industrial & Engineering Chemistry Research*, 32(12):3006–3013, 1993.
- [11] R.C. Hurlbert and J.O. Konecny. Diffusion of Hydrogen through Palladium. *The Journal of Chemical Physics*, 34(2):655–658, 1961.
- [12] M. Mulder. *Basic Principles of Membrane Technology*. Kluwer Academic, 1996.
- [13] A. Sieverts. Die aufnahme von gasen durch metalle. *Zeitschrift Fr Met.*, 21:37–46, 1929.
- [14] R. Burch and N.B. Francis. Pressure against composition isotherms and thermodynamic data for the α -phase of the palladium/hydrogen system. *J. Chem. Soc., Faraday Trans. 1*, 69:1978–1982, 1973.
- [15] M.J.B. Evans. Surface Area Effects on the Sorption of Hydrogen by Palladium. *Canadian Journal of Chemistry*, 52(7):1200–1205, 1974.

- [16] G. L. Holleck. Diffusion and solubility of hydrogen in palladium and palladium–silver alloys. *The Journal of Physical Chemistry*, 74(3):503–511, 1970.
- [17] Y. Sakamoto, S. Hirata, and H. Nishikawa. Diffusivity and solubility of hydrogen in Pd-Ag and Pd-Au alloys. *Journal of the Less Common Metals*, 88(2):387 – 395, 1982.
- [18] S. Uemiya, T.i Matsuda, and E. Kikuchi. Hydrogen permeable palladium-silver alloy membrane supported on porous ceramics. *Journal of Membrane Science*, 56(3):315 – 325, 1991.
- [19] D.L. McKinley. Metal alloy for hydrogen separation and purification, 1967. US Patent 3,350,845.
- [20] The Purification of Hydrogen: A review of the technology emphasising the current status of palladium membrane diffusion. *Platinum Metals Review*.
- [21] A.K.M. Fazle Kibria and Y. Sakamoto. The effect of alloying of palladium with silver and rhodium on the hydrogen solubility, miscibility gap and hysteresis. *International Journal of Hydrogen Energy*, 25(9):853 – 859, 2000.
- [22] F. Scura, G.Barbieri, and E. Drioli. H₂ for PEM-FC: effect of CO in the purification by means of Pd-based membranes . *Desalination*, 200(13):239 – 241, 2006.
- [23] H. Amandusson, L.-G. Ekedahl, and H. Dannetun. The effect of CO and O₂ on hydrogen permeation through a palladium membrane. *Applied Surface Science*, 153(4):259 – 267, 2000.
- [24] A.L. Mejdell, M. Jndahl, T.A. Peters, R. Bredesen, and H.J. Venvik. Effects of CO and CO₂ on hydrogen permeation through a 3m Pd/Ag 23wt.% membrane employed in a microchannel membrane configuration. *Separation and Purification Technology*, 68(2):178 – 184, 2009.
- [25] F. Gallucci, F. Chiaravalloti, S. Tosti, E. Drioli, and A. Basile. The effect of mixture gas on hydrogen permeation through a palladium membrane: Experimental study and theoretical approach. *International Journal of Hydrogen Energy*, 32(12):1837 – 1845, 2007.
- [26] M. Eriksson and L.-G Ekedahl. Real time measurements of hydrogen desorption and absorption during CO exposures of Pd: hydrogen sticking and dissolution. *Applied Surface Science*, 133(12):89 – 97, 1998.
- [27] M.M. Wolf, H. Zhu, W.H. Green, and G.S. Jackson. Kinetic model for polycrystalline Pd/PdOx in oxidation/reduction cycles. *Applied Catalysis A: General*, 244(2):323 – 340, 2003.
- [28] A.L. Mejdell, H. Klette, A. Ramachandran, A. Borg, and R. Bredesen. Hydrogen permeation of thin, free-standing Pd/Ag23 % membranes before and after heat treatment in air. *Journal of Membrane Science*, 307(1):96 – 104, 2008.
- [29] S.K. Gade, P. M. Thoen, and J.D. Way. Unsupported palladium alloy foil membranes fabricated by electroless plating. *Journal of Membrane Science*, 316(12):112 – 118, 2008.
- [30] D. Fort, J.P.G. Farr, and I.R. Harris. A comparison of palladium-silver and palladium-yttrium alloys as hydrogen separation membranes. *Journal of the Less Common Metals*, 39(2):293 – 308, 1975.

- [31] L. Yang, Z. Zhang, B. Yao, X. Gao, H. Sakai, and T. Takahashi. Hydrogen permeance and surface states of Pd-Ag/ceramic composite membranes. *AIChE Journal*, 52(8):2783–2791, 2006.
- [32] K. Zhang, S.K. Gade, Ø. Hatlevik, and J.D. Way. A sorption rate hypothesis for the increase in H₂ permeability of palladium-silver (PdAg) membranes caused by air oxidation. *International Journal of Hydrogen Energy*, 37(1):583 – 593, 2012. 11th China Hydrogen Energy Conference.
- [33] A. Ramachandran, W.M. Tucho, A.L. Mejdell, M. Stange, H.J. Venvik, J.C. Walmsley, R. Holmestad, R. Bredesen, and A. Borg. Surface characterization of Pd/Ag23.wt% membranes after different thermal treatments. *Applied Surface Science*, 256(20):6121 – 6132, 2010.
- [34] W.M. Tucho, H.J. Venvik, J.C. Walmsley, M. Stange, A. Ramachandran, R.H. Mathiesen, A. Borg, R. Bredesen, and R. Holmestad. Microstructural studies of self-supported (1.510 m) Pd/23 wt%Ag hydrogen separation membranes subjected to different heat treatments. *Journal of Material Science*, 44(16):4429–442, 2009.
- [35] A.L. Mejdell, D. Chen, T.A. Peters, R. Bredesen, and H.J. Venvik. The effect of heat treatment in air on CO inhibition of a 3µm Pd/Agwt.% membrane. (Unpublished), 2009.
- [36] T.A. Peters, M. Stange, and R. Bredesen. On the high pressure performance of thin supported Pd23%Ag membranes - Evidence of ultrahigh hydrogen flux after air treatment. *Journal of Membrane Science*, 378(12):28 – 34, 2011. Membranes for a Sustainable Future Section.
- [37] N. Vicinanza, I.-H. Svenum, T.A. Peters, R. Bredesen, and H.J. Venvik. New insight to the heat treatment in air procedure for enhancement of the hydrogen transport properties of thin Pd77%Ag23% membranes. (Unpublished), (2014).
- [38] I.-H. Svenum, J.A. Herron, M. Mavrikakis, and H.J. Venvik. Adsorbate-induced segregation in a PdAg membrane model system: Pd₃Ag(1 1 1). *Catalysis Today*, 193(1):111 – 119, 2012.
- [39] H.K. Dipojono, A.A.B. Padama, N. Ozawa, H. Nakanishi, and H. Kasai. A First Principles Study on Dissociation and Adsorption Processes of H₂ on Pd 3 Ag(111) Surface. *Japanese Journal of Applied Physics*, 49(11R):115702, 2010.
- [40] J.K. Ali, E.J. Newson, and D.W.T. Rippin. Deactivation and regeneration of Pd/Ag membranes for dehydrogenation reactions. *Journal of Membrane Science*, 89(12):171 – 184, 1994.
- [41] M. Amano, C.Nishimura, and M. Komaki. Effects of high concentration co and co₂ on hydrogen permeation through the palladium membrane. *Materials Transactions, JIM*, 31:404, 1990.
- [42] D.P. Broom. Hydrogen sorption measurements on potential storage materials: experimental methods and measurement accuracy. EUR 23242 EN. *Office for Official Publications of the European Communities, Luxembourg*, 2008.
- [43] H. Hertz. *Annalen der Physik*, 267(8):983, 1887.
- [44] A. Einstein. *Annalen der Physik*, 322(6):132, 1905.

- [45] K. Siegbahn, C. Nordling, A. Fahlman, R. Nordberg, K. Hamrin, J. Hedman, G. Johansson, T. Bergmark, S.-E. Karlsson, and I. Lindgren. volume 20.
- [46] H.J. Venvik. *Adsorbates on cobalt and platinum single crystal surfaces studied by STM*. PhD thesis, Norwegian University of Science and Technology, 1998.
- [47] D.P. Woodruff and T.A. Delchar. *Modern Techniques of Surface Science* -, volume -Second Edition. New York: Cambridge University Press.
- [48] A. Zangwill. *Basic Principles of Membrane Technology*. Cambridge: Cambridge University Press, 1988.
- [49] T.N. Rhodin and J. Gadzuk. *The Nature of the Surface Chemical Bond*. New York: North-Holland Pub. Co., 1979.
- [50] D.R. Penn. Quantitative chemical analysis by {ESCA} . *Journal of Electron Spectroscopy and Related Phenomena*, 9(1):29 – 40, 1976.
- [51] H. Klette and R. Bredeesen. Sputtering of very thin palladium-alloy hydrogen separation membranes. *Membrane Technology*, 2005(5):7 – 9, 2005.
- [52] N. Vicinanza, L.N. Nss, I.-H. Svenum, T.A. Peters, R. Bredeesen, A. Borg, and H.J. Venvik. Thickness dependent effects of solubility and surface phenomena on hydrogen transport properties of sputtered Pd77%Ag23% thin film membranes. (Unpublished), (2014).
- [53] N. Itoh and W.-C. Xu. Selective hydrogenation of phenol to cyclohexanone using palladium-based membranes as catalysts. *Applied Catalysis A: General*, 107(1):83 – 100, 1993.
- [54] K. Hou and R. Hughes. The effect of external mass transfer, competitive adsorption and coking on hydrogen permeation through thin Pd/Ag membranes. *Journal of Membrane Science*, 206(12):119 – 130, 2002.
- [55] H. Li, A. Goldbach, W. Li, and H. Xu. PdC formation in ultra-thin Pd membranes during separation of H₂/CO mixtures. *Journal of Membrane Science*, 299(12):130 – 137, 2007.
- [56] A.L. Mejdell, M. Jøndahl, T.A. Peters, and H.J. Venvik. Experimental investigation of a microchannel membrane configuration with a 1.4m Pd/Ag23wt.% membrane- Effects of flow and pressure. *Journal of Membrane Science*, 372:6–10, 2009.
- [57] O.M. Løvvik and R.A. Olsen. Density functional calculations of hydrogen adsorption on palladiumsilver alloy surfaces. *The Journal of Chemical Physics*, 118(7), 2003.
- [58] G. Barbieri, F. Scura, F. Lentini, G. De Luca, and E. Drioli. A novel model equation for the permeation of hydrogen in mixture with carbon monoxide through PdAg membranes . *Separation and Purification Technology*, 61(2):217 – 224, 2008.
- [59] L.E. Walle, H. Grnbeck, V.R. Fernandes, S. Blomberg, M.H. Farstad, K. Schulte, J. Gustafson, J.N. Andersen, E. Lundgren, and A. Borg. Surface composition of clean and oxidized Pd75Ag25(100) from photoelectron spectroscopy and density functional theory calculations. *Surface Science*, 606(2324):1777 – 1782, 2012.

- [60] L. Yang, Z. Zhang, X. Gao, Y. Guo, B. Wang, O. Sakai, H. Sakai, and T. Takahashi. Changes in hydrogen permeability and surface state of PdAg/ceramic composite membranes after thermal treatment. *Journal of Membrane Science*, 252(12):145 – 154, 2005.

Abbreviations

Symbol	Description
AFM	Atomic force microscopy
Ag	Silver
Al	Alumina
C	Carbon
CH ₄	Methane
CO	Carbon monoxide
CO ₂	Carbon dioxide
GC	Gas chromatography
H	Atomic hydrogen
H ₂	Hydrogen
H ₂ O	Water
HTA	Heat treatment in air
LFC	Liquid flow controller
MFC	Mass flow controller
Mg	Magnesium
MSR	Methane steam reforming
N ₂	Nitrogen
O	Oxygen
Pd	Palladium
rds	Rate determining step
S	Sulphur
Si	Silicon
TEM	Transmission electron microscopy
WGSR	Water gas shift reaction
XPS	X-ray photoelectron spectroscopy
XRD	X-ray diffraction

Symbols



Symbol	Description	Units
D	Diffusion coefficient	[m ⁻² s ⁻¹]
D ₀	Pre-exponential factor of diffusion	[m ⁻² s ⁻¹]
E _a	Activation energy	[J mol ⁻¹]
E	Energy	[J mol ⁻¹]
ΔH	Enthalpy change	[J mol ⁻¹]
hν	Photon energy	[J mol ⁻¹]
I	Peak intensity	[-]
J	Flux	[mol m ⁻² s ⁻¹]
K _S	Solubility constant	[mol m ⁻³ Pa ^{-0.5}]

k	Adsorption/desorption constant	[-]
K	Equilibrium constant	[-]
n	Coordination number	[-]
P	Permeability	[mol m m ⁻² s ⁻¹ Pa ^{-0.5}]
P	Pressure	[bar]
p	Partial pressure	[Pa]
Φ_S	Work function	[J mol ⁻¹]
R	Gas constant	[J K ⁻¹ mol ⁻¹]
ΔS	Entropy change	[J mol ⁻¹ K ⁻¹]
t	Membrane thickness	[m]
T	Temperature	[K]
Θ	Surface coverage	[-]
V	Volume	[L]

Appendices

A Risk Analysis

side 1 av 1 03.10.2013

NTNU	Hazardous activity identification process				Risikovuordering	Nummer	Dato	
					HMS-avd.	HMSRV2801		
HMS					Godkjent av	Side	Erstatter	

Unit: Kjemisk prosesssteknologi Date: 27.09.2013

Line manager: Edd Blekkan


Participants in the identification process (including their function):

Hilde Venvik (supervisor), Nicla Vicinanza (co-supervisor), Karin Dragsten (staff engineers, instrument responsible), Bengt Arild Johannesen (MSc)

Short description of the main activity/main process:

Chemisorption instruments, Micromeritics ASAP 2020/2010

ID no.	Activity/process	Responsible person	Laws, regulations etc.	Existing documentation	Existing safety measures	Comment
1	Use of flammable and toxic gasses (H ₂ , CO).	Room responsible/instrument responsible/user	AML	MSDS, user manual	Perform leak tests when replacing gas bottles or changing the gas feed system. Detection system	Training is compulsory before changing gas bottles and performing changes in the feed system. CO bottle should be closed when not in use.
2	Oven		AML	User manual (blue folder)	Warning sign and shield	Cool down sample reactor before disconnecting it.
3	Liquid (N ₂)	User	AML	MSDS, user manual	Danger note in the lab, personal protective equipment available in lab. Trolley with tip. User must have training	

NTNU		Risk assessment		Utarbeidet av		Nummer		Dato	
				HMS-avd.		HMSRV2603		04.02.2011	
HMS /KS				Godkjent av		Side		Erstatler	



Unit: Kjemisk prosesseteknologi Date: 27.09.2013
 Line manager: Edd Blekkan



Participants in the identification process (including their function):
Hilde Vervik (supervisor), Nicola Vicinanza (co-supervisor), Karin Dragsten (staff engineers, instrument responsible), Bengt Arild Johannesen (MSc)

Signatures: *Hilde Vervik*

ID no.	Activity from the identification process form	Potential undesirable incident/strain	Likelihood:		Consequence:				Risk value	Comments/status Suggested measures
			Likelihood (1-5)	Human (A-E)	Human (A-E)	Environment (A-E)	Economy/material (A-E)	Reputation (A-E)		
1	Use of flammable and toxic gasses (H ₂ , CO).	Poisoning/fire/explosion	2	B					2B	Gas detection system in the lab. Changing of the gas bottle will be done by the staff engineer or
2	Oven	Skin burn, fire	2	B					2B	Warning sign on the oven
3	Liquid (N ₂)	skin irritation, eye contact	2	D					2D	Danger note in the lab, personal protective equipment available in lab. Trolley with tip. User must have training

Operating Instructions

Instrument/Apparatus: Micromeritics ASAP 2020/2010		
Serial Number:	Placement K5-441	
Original Manual:	Blue folder/white folder placed beside instrument	
Log book with signature for training & maintenance:		
Log book beside the instrument		
Risk Evaluation		
Date: 17.08.2013		
Archived:		
Compulsory Protection Equipment:	Hazards:	
Safety Goggles	<input checked="" type="checkbox"/>	Fire <input checked="" type="checkbox"/>
Gloves	<input checked="" type="checkbox"/>	Chemicals/Gasses <input checked="" type="checkbox"/>
Hearing Protection	<input type="checkbox"/>	Electricity/Power <input type="checkbox"/>
Protective Clothing	<input checked="" type="checkbox"/>	Temperature/Pressure <input checked="" type="checkbox"/>
Breathing Protection	<input type="checkbox"/>	Cutting/Crushing <input type="checkbox"/>
Shielding	<input checked="" type="checkbox"/>	Rotating Equipment <input type="checkbox"/>
Other	<input type="checkbox"/>	Hazardous Waste <input type="checkbox"/>
None	<input type="checkbox"/>	Beyond regular working hours <input checked="" type="checkbox"/>
		Others <input type="checkbox"/>
		None <input type="checkbox"/>
Operating Instructions		
(Fill In or Attach Seperate Instructions)		
Detailed instructions in the user manual beside the instrument. User instruction/procedure beside the instrument. All users will have a copy of these precedures.		
Emergency Procedure		
(Emergency Stop Procedure, Image of Switches/Stop Procedure):		
Close the gas bottles and turn of the electricity, main switch on the side. The gas bottles belonging to the instrument are marked with ASAP.		
Maintenance Routines		
Frequency When needed		
Service Agreements: Once a year		
Maintenance Contact: Mikrotek, Tom Andre Brubak 90838670/ brubak@microtek.no		
Mainteinans described in the procedure		
Equipment Responsible:	Deputy:	
Name: Karin Dragsten	Name: Magnus Rønning	
Telephone 91897245	Telephone 94121	
Mobile: 48023837	Mobile:	
Signature:	Signature:	
Controlled & Updated:		
Date:	Date:	Date:
Date:	Date:	Date:


		Hazardous activity identification process			
				Numme HMSRV 2601	
		Risikovurdering HMS-avd.		Dato 26.09.2013	
		Godkjent av		Erstatler	


Unit: Kjemisk prosesseteknologi Date: 26.09.2013
 Line manager: Edd. A. Blekkan

Participants in the identification process (including their function):
Hilde Venvik (supervisor), Nicla Vicinanza (PhD stipendiat), Bengt Arild Johannessen

Short description of the main activity/main process:

Membrane apparatus

ID no.	Activity/process	Responsible person	Laws, regulations etc.	Existing documentation	Existing safety measures	Comment
1	Assembling/use of flammable gases H ₂ /CH ₄	Hilde Venvik		safety data sheet EIGA067A (H ₂) no number (CH ₄)	Room detector, local detector, leak testing, gloves, goggles, lab coat.	
2	Assembling/use of toxic gases CO	Hilde Venvik		safety data sheet: no number	Room detector, local detector, leak testing, gloves, goggles, lab coat.	
3	Assembling/use of non toxic and inert gases: CO ₂ /N ₂ /Ar/He	Hilde Venvik		number CO ₂ ; EIGA089A N ₂ ; EIGA003A Ar; EIGA061A He	Room detector, local detector, leak testing, gloves, goggles, lab coat.	Change of gas bottles is done by appropriate staff within working hours
4	Use of ethanol for cleaning procedures	Hilde Venvik		safety data sheet: no number	Gloves, lab coat, goggles.	
5	Use of acetone for cleaning procedures	Hilde Venvik		safety data sheet: no number	Gloves, lab coat, goggles. insulation tape, special gloves	
6	Use of heating tape	Hilde Venvik	Arbeidsmiljø loven	None		

		<h3>Risk assessment</h3>			
Utarbeidet av	Nummer	Dato			
HMS-avd.	HMSRV2603	26.09.2013			
Godkjent av	Side	Erstatter			

Unit: Kjemisk prosesseteknologi Date: 26.09.2013
 Line manager: Edd A. Blekken
 Participants in the identification process (including their function): Hilde Vennik (supervisor), Nicla Vicinanza (PhD stipendiat), Bengt Arild Johannesen

Signatures: 

ID no.	Activity from the identification process form	Potential undesirable incident/strain	Likelihood: Likelihood (1-5)	Consequence:			Risk value	Comments/status Suggested measures
				Human (A-E)	Environment (A-E)	Economy/material (A-E)		
1	Assembling/use of flammable gases H ₂ /CH ₄	(a) leakage (b) fire	(a) 3 (b) 1	(a) A (b) D	(a) A (b) D	(a) A (b) D	(a) A3 (b) D1	Leak testing with noble gases and room and local
2	Assembling/use of toxic gases CO	(a) leakage (b) fire	(a) 3 (b) 1	(a) D/E (b) D	(a) A (b) D	(a) A (b) D	(a) D/E3 (b) D1	Leak testing with noble gases and room and local
3	Assembling/use of non toxic and inert gases: CO ₂ /N ₂ /Ar/He	(a) leakage	(a) 3	(a) B	(a) A	(a) A	(a) B3	testing with noble
4	Use of ethanol for cleaning procedures	(a) spill (b) fire	(a) 3 (b) 1	(a) A (b) C	(a) A (b) C	(a) A (b) C	(a) A3 (b) C1	Use of gloves, lab coat, goggles.
5	Use of acetone for cleaning procedures	(a) spill (b) fire	(a) 3 (b) 1	(a) B (b) C	(a) A (b) C	(a) A (b) C	(a) B3 (b) C1	Use of gloves, lab coat, goggles.
6	Use of heating tape	(a) short circuit (b) burn	(a) 1 (b) 2	(a) C/D (b) B	(a) A (b) A	(a) A (b) A	(a) C/D1 (b) B2	Use of insulation tape, special gloves,

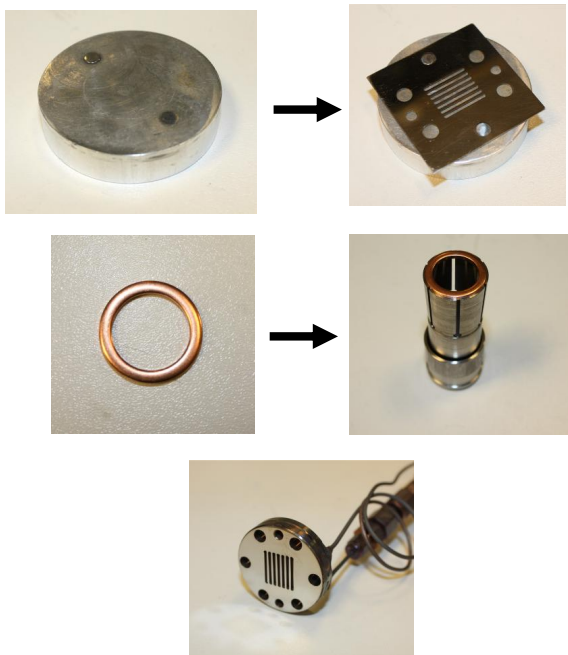
Operating Instructions

Instrument/Apparatus: Membrane apparatus		
Serial Number: None	Placement Kjemihall D 2nd floor	
Original Manual: None		
Log book with signature for training & maintenance: None		
Risk Evaluation		
Date: 27/09/2011		
Archived:		
Compulsory Protection Equipment:	Hazards:	
Safety Goggles	<input checked="" type="checkbox"/> Fire	<input checked="" type="checkbox"/>
Gloves	<input checked="" type="checkbox"/> Chemicals/Gasses	<input checked="" type="checkbox"/>
Hearing Protection	<input type="checkbox"/> Electricity/Power	<input checked="" type="checkbox"/>
Protective Clothing	<input checked="" type="checkbox"/> Temperature/Pressure	<input checked="" type="checkbox"/>
Breathing Protection	<input type="checkbox"/> Cutting/Crushing	<input type="checkbox"/>
Shielding	<input type="checkbox"/> Rotating Equipment	<input type="checkbox"/>
Other	<input checked="" type="checkbox"/> Hazardous Waste	<input checked="" type="checkbox"/>
None	<input type="checkbox"/> Beyond regular working hours	<input checked="" type="checkbox"/>
	<input type="checkbox"/> Others	<input checked="" type="checkbox"/>
	<input type="checkbox"/> None	<input type="checkbox"/>
Operating Instructions		
(Fill In or Attach Seperate Instructions)		
GC manual; Eurothermal manual; HSE - course; leak testing before every experiment.		
Emergency Procedure		
(Emergency Stop Procedure, Image of Switches/Stop Procedure):		
Shut down gas bottles and cut power. Then evacuate.		
Maintenance Routines		
Frequency When needed		
Service Agreements: None		
Maintenance Contact: None		
Maintenance Describe: None outside maintenance.		
Equipment Responsible:		Deputy:
Name: Hilde Venvik	Telephone:	Name: Nicla Vicinanza
Mobile: 92808787	Signature:	Telephone 7359411
		Mobile: 47166722
		Signature:
Controlled & Updated:		
Date:	Date:	Date:
Date:	Date:	Date:

B Membrane Module Mounting

Polishing

Polish the feed side of the module and the channel in "Sliperom". Use 1200, 2400 and finally 4000 polishing disc. Polish the copper gasket as well with 2400 polishing disc to ensure that the sealing is efficient. A new copper gasket is used for every new module.



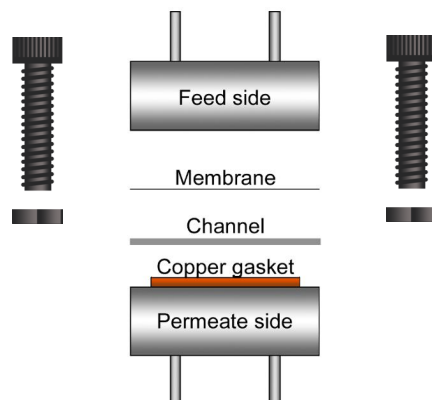
Cleaning

Pour some ethanol in a beaker then put the beaker in the ultrasound bath. Put both feed and permeate side of the module in ethanol. Let it run for about 10 minutes.

Dry out most of the ethanol from the parts with compressed air, and connect one at a time each tube of the module to the argon tap on the wall to dry the inside of the pipes:

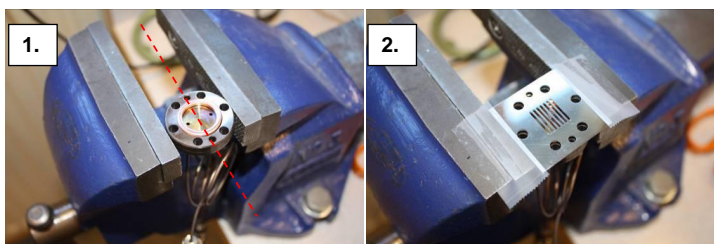
Assembling the module

The whole module is built-up as shown on this scheme:



1. First, mount the permeate side of the module and the copper gasket on the vice as depicted below, trying to align the smaller holes with the edge of the vice so that the screw holes are easier to find later on.

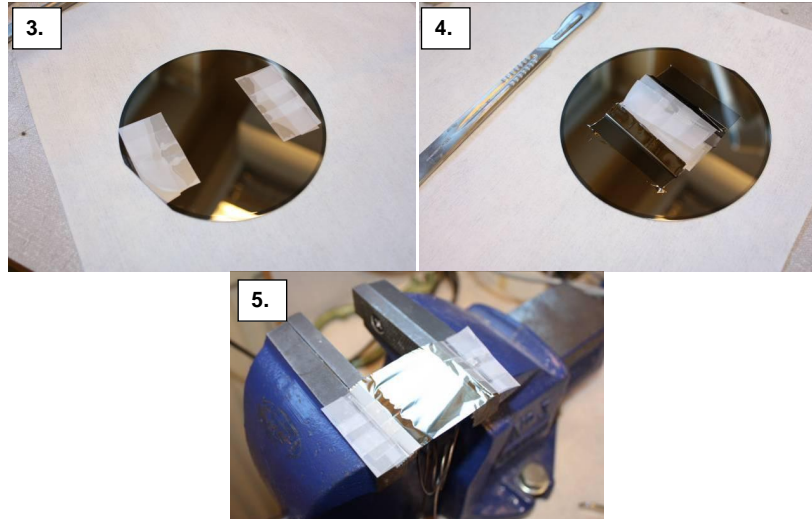
2. Put the channel on top and tape it to the vice.



3. Then cut away the membrane from the as-sputtered wafer. Put gloves on and put the wafer with film side up on a dust-free paper. Prepare tape bits approximately the size of the channel side, forming little handles. Stick them on the film so that the tape-free area is approximately that of the channel area and leave some sticky surface free so that it can be stuck on top of the vice.

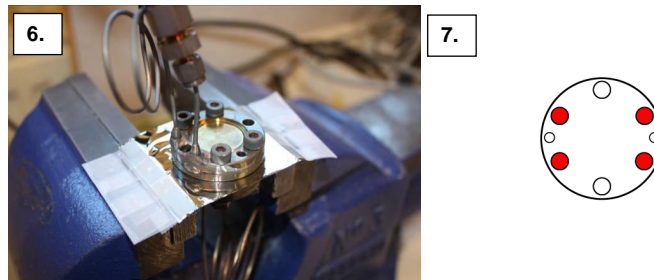
4. Cut along all edges with a scalpel. Pull away the membrane from one side then from the other side. Pulling from one side only can cause the film to rip from where the other piece of tape is stuck.

5. Lay the film on the channel trying to make it sit flat.



6. Cover it with the feed side of the module. Align it by looking from the sides. If possible, hold the upper tubes by hand or gallows, at least at first, to avoid wrinkling the film. Pierce the first hole with a pointy object like tweezers not to crack the film any further. Put a screw in and drive a bolt on.

7. Repeat this operation for these other holes.



8. Cut away the surplus of film, not too close to the screws area so it does not tear apart. Peel away any remaining tape bit.

9. Screw the bolts on evenly. Undo the vice and rotate the whole module. Tighten the vice and put the last screws in. Screw all the bolts as tight as possible with a hex key and a no. 6 wrench; screws will tend to come loose overtime with high

temperatures. Use force on the wrench not to break the key. Connect the pipes to set-up.



Unmounting a module after testing

After testing, leave the support feed gas (N_2) and sweep gas (Ar) only and shut the rest of the valves on the set-up. Remaining hydrogen should be swept away for about 1 hour at high temperature ($300^\circ C$ or over).

The module should then be cooled down to room temperature. Apply a downward temperature ramp with the oven controller and take the fibreglass rolls off the oven.

Once at room temperature, put the N_2 and Ar controller setpoints to 0.0 in LabView / MiniLab and close switches on the set-up.

Undo pipe bolts on the module and unscrew all six bolts. Pick up the copper gasket with pliers.

C Mass Flow Controller Calibration

The mass flow controllers were calibrated by checking correlation of set-points and flowrates. The set-points used were in the range of 5 - 95%. The data from the calibrations as well as the calibration curves are given in below.

Set Point [%]	Time [s]	Volume [ml]	Flowrate [ml/min]
5	518.76	100	37.79
15	51.28	100	117.02
30	25.49	100	235.36
50	30.26	200	396.56
70	21.61	200	555.38
85	17.76	200	675.80
95	16.00	200	750.00

Table A1: Calibration data for the H_2 MFC

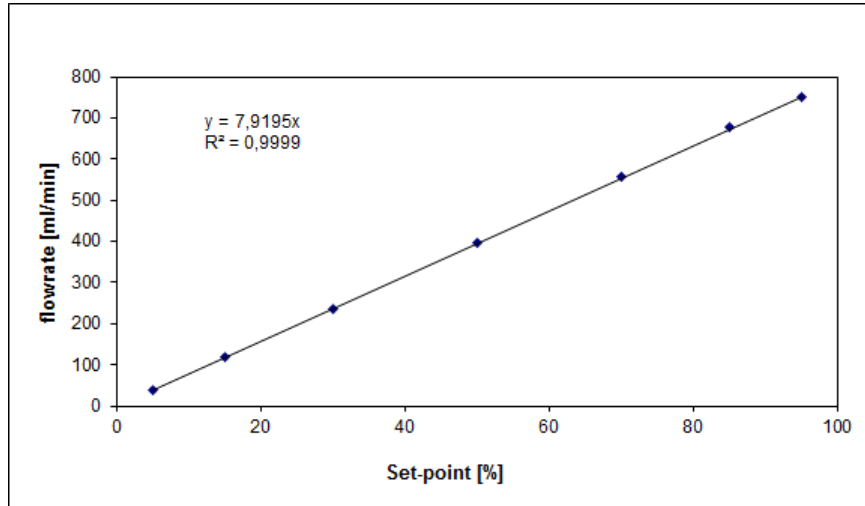


Figure A1: Calibration Curve of H_2

Set Point [%]	Time [s]	Volume [ml]	Flowrate [ml/min]
50	209.35	200	57.32
70	149.61	200	80.21
90	110.18	200	108.91

Table A2: Calibration data for the N_2 MFC

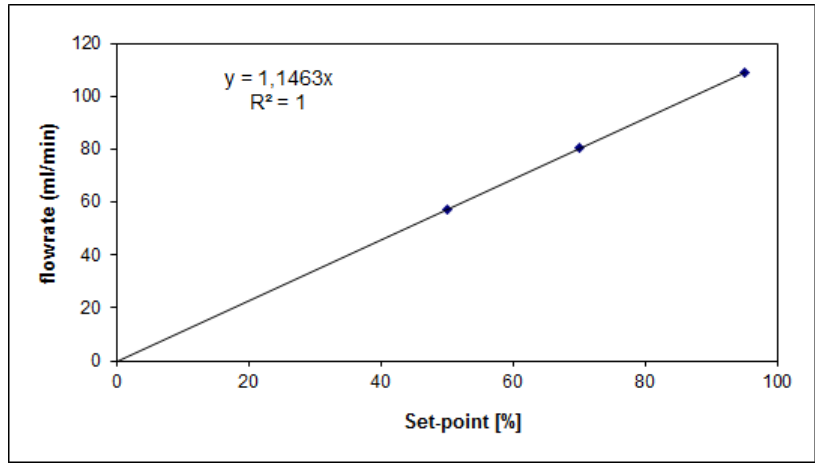


Figure A2: Calibration Curve of N_2 MFC

Set Point [%]	Time [s]	Volume [ml]	Flowrate [ml/min]
30	51.84	200	231.50
50	30.59	200	392.32
70	21.70	200	553.12
90	15.97	200	751.41

Table A3: Calibration data for the second H_2 MFC

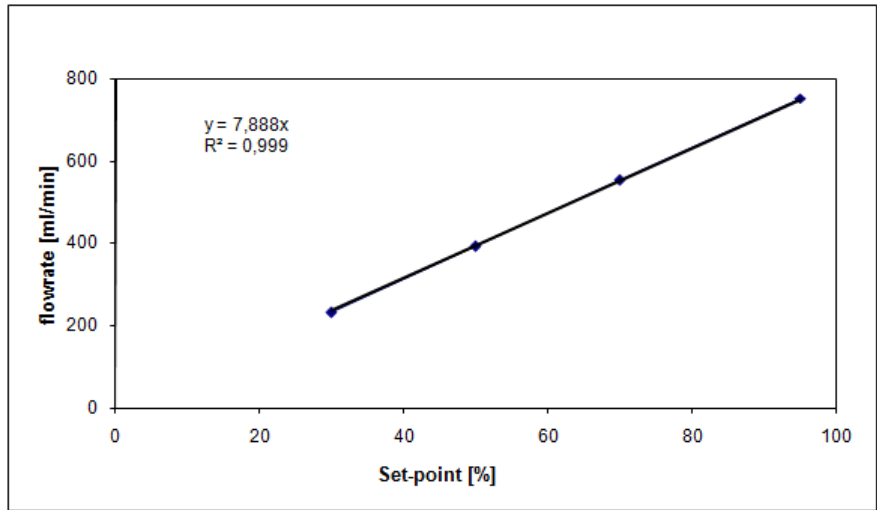


Figure A3: Calibration Curve of the second H_2 MFC

Set Point [%]	Time [s]	Volume [ml]	Flowrate [ml/min]
5	7.77	9	69.50
15	25.28	90	213.61
30	12.45	90	433.74
50	7.43	90	726.78
70	5.16	90	1046.51
85	4.28	90	1261.68
95	3.78	90	1428.57

Table A4: Calibration data for the *Ar* MFC

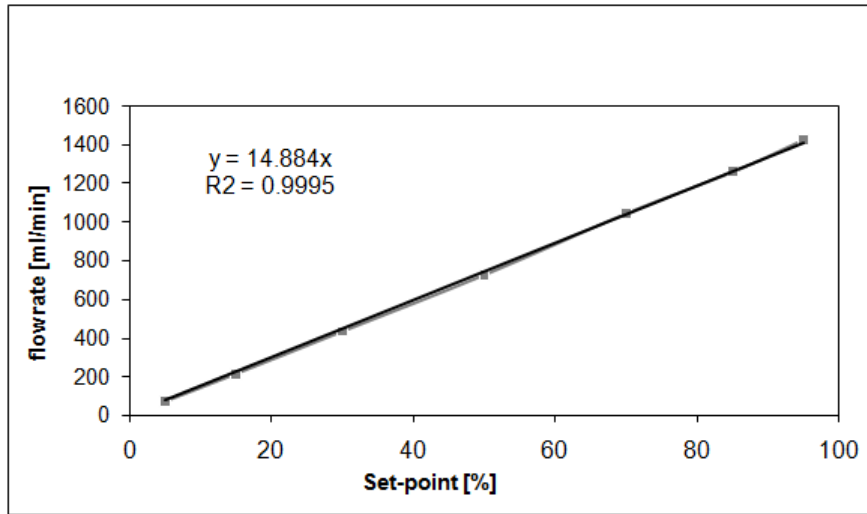


Figure A4: Calibration Curve of the *Ar* MFC

Set Point [%]	Time [s]	Volume [ml]	Flowrate [ml/min]
40	664.81	100	9.02
70	379.28	100	15.82
95	271.13	100	21.34

Table A5: Calibration data for the *CO* MFC

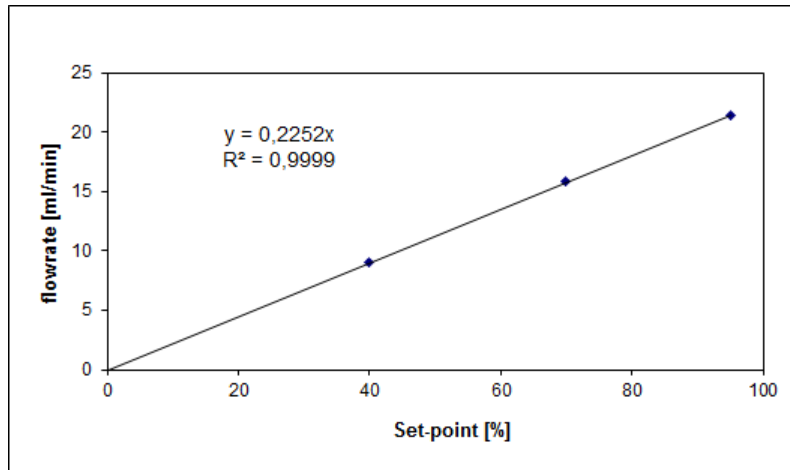


Figure A5: Calibration curve of *CO* MFC

D Micro-GC Calibration

Micro-GC was utilized in this work for several reasons. Retentate flow was examined in order to validate that membrane was intact after mounting. Permeate and retentate flow were checked to determine the gases present on respective sides during experiment. Hydrogen flow on permeate stream was monitored for long term experiments. A calibration of the micro-GC was performed by the following ways:

1. Identification of components and fractions from gas mixture set with calibrated MFCs.
 2. Identification of components and fractions from calibration gas
 3. Quantification of hydrogen gas flow compared to calibrated MFC flow.
1. Table A6 shows identification of components and respective fractions, where gas mixture was set with calibrated MFCs.

Table A6: Detection of components by Micro-GC, and their respective fraction with 200NmL total flow

Component	Set point fraction [%]	Determined fraction [%]
H ₂	47.0	46.5
N ₂	47.0	49.8
CO	5.0	3.7
CO ₂	1.0	0.1

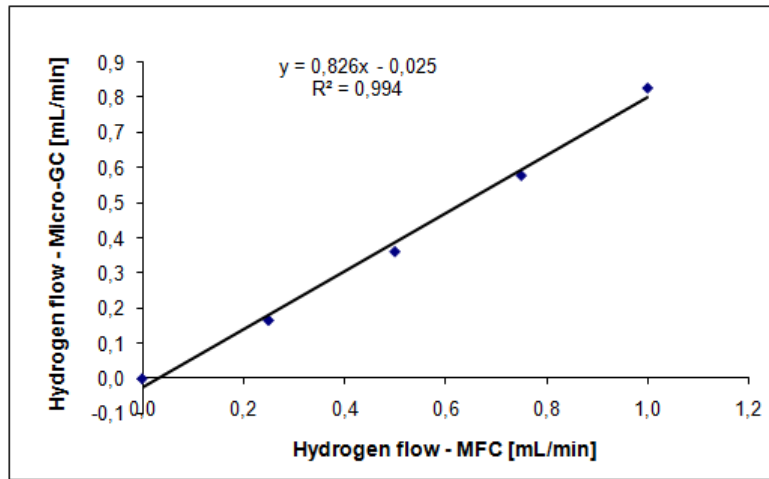
2. Table A7 shows identification of components and respective fractions, from a calibration gas bottle.

Table A7: Detection of components by Micro-GC, and their respective fraction from calibration gas bottle.

Component	Set point fraction [%]	Determined fraction [%]
N ₂	86.0	78.2
H ₂	10.0	16.3
CO	1.0	2.1
CO ₂	1.0	3.1
He	1.0	0.3
CH ₄	1.0	0.0

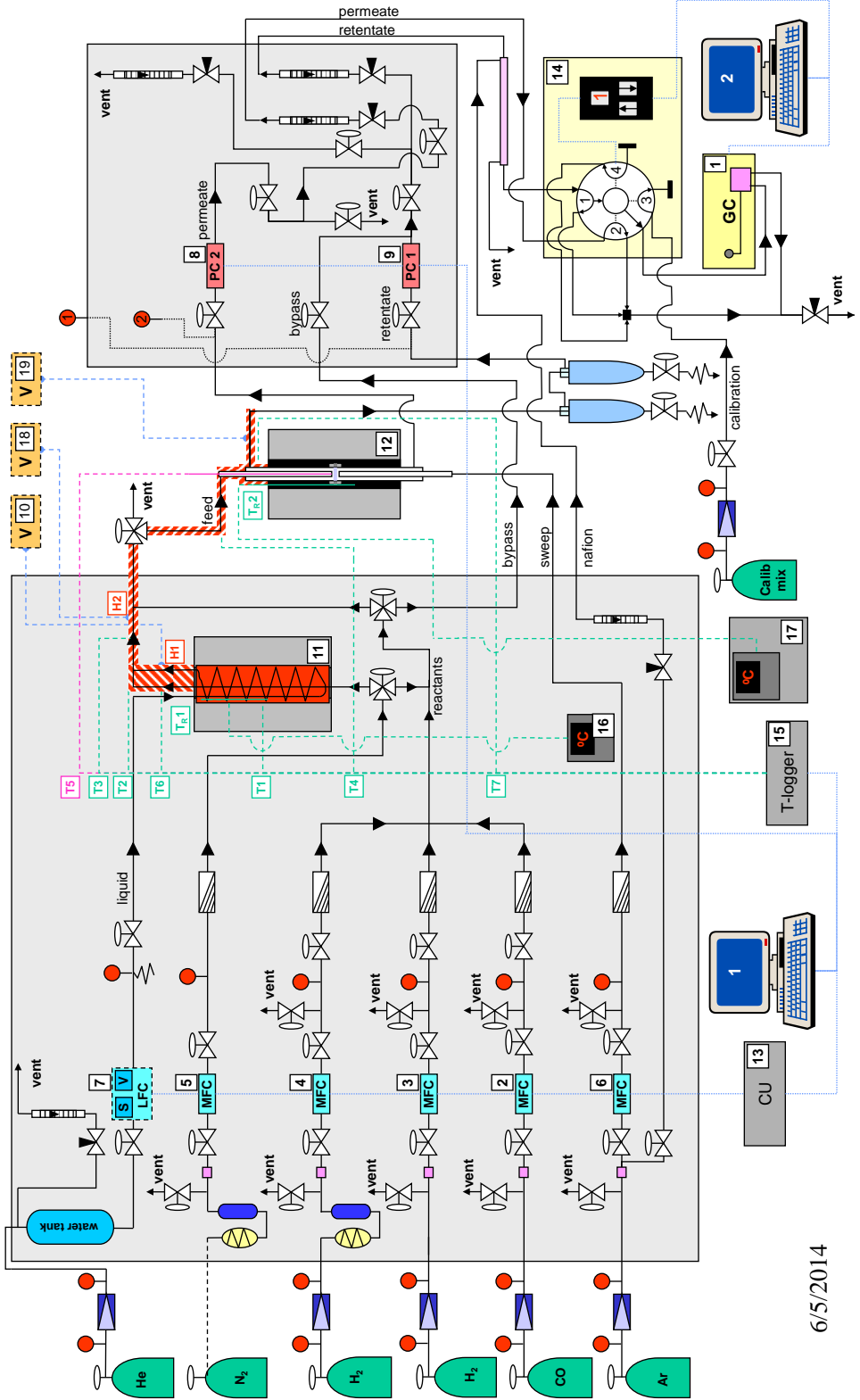
3. Figure A6 shows calibration of Micro-GC with the aspect of hydrogen gas flow quantification by Micro-GC, compared to a flow set by calibrated MFC.

Figure A6: Calibration Curve of H_2 flow detected by Micro-GC by calibrated MFC.





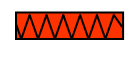

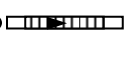
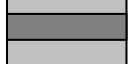


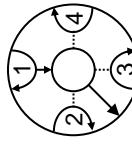














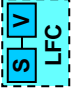

E Membrane Reactor Setup Flowsheet

Catalytic membrane reactor laboratory



6/5/2014

FLOW SHEET SYMBOL LIST

	hoke valve		condensing tank		evaporator
	three-way valve		flow indicator (rotameter)		oven
	needle valve		heated lines (heating tape) with thermocouple		4-port valve
	reduction valve		Voltron effect regulator		Eurotherm
	one-way valve		nafion dryer		
	relief valve		micro heat exchanger		
	pressure indicator		T or micro mixer		
	gas drier		dp-cell		
	oxy-trap				
	particle filter				
	mass flow controller				
	liquid flow controller with Sensor and Valve				
	pressure controller (< 8 bar)				

F Lifespan of Membrane over experiments 2a-2f

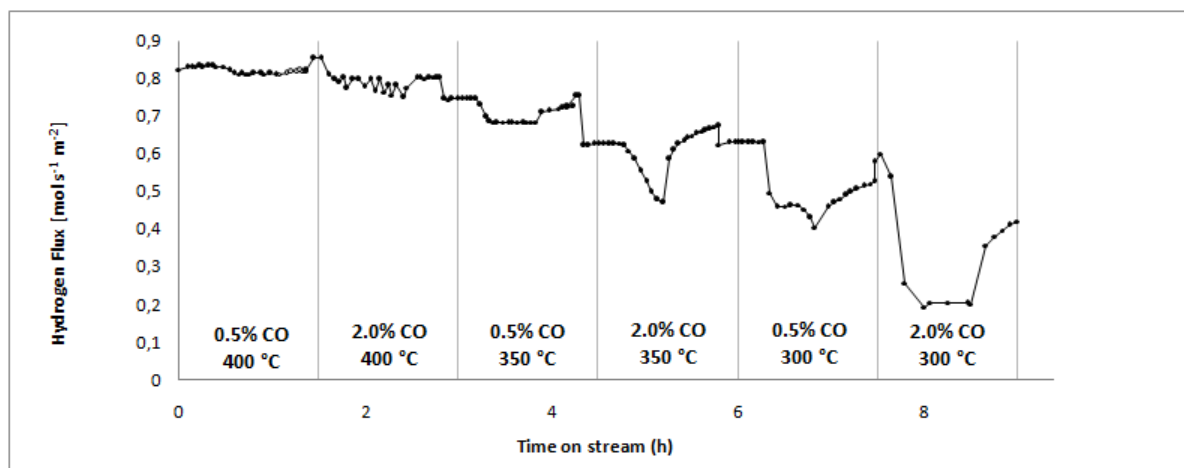


Figure A7: Hydrogen flux over experiment 2a-2f conducted.

G Liquid Flow Controller Calibration

The liquid flow controller was calibrated by checking correlation of set-points and flowrates. This was done by weighing mass of water after approximately 6 minutes at different set points. The set-points used were 100, 75 and 50, and three parallels were done at each set point. This range was chosen as the LFC range was very small, and lower amounts could possibly lead to more evaporation from sample. Calibration is given in table and figure below.

Set point [%]	Set point flow [g/hr]	Determined flowrate [g/hr]
100	2.00	1.92
75	1.50	1.40
50	1.00	0.86

Table A8: Calibration data for the H₂O LFC

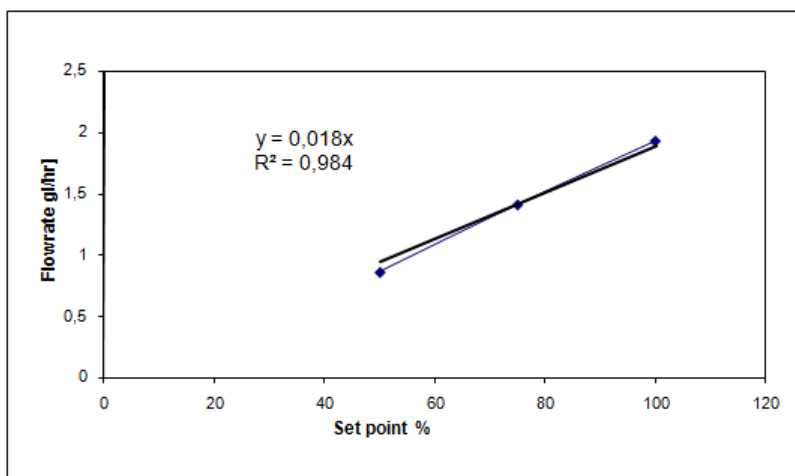


Figure A8: Calibration Curve of H₂O

H Volumetric Sorption Apparatus Sequence

Table A9: Apparatus sequence of sorption measurements performed at 350°C.

Task	Gas	Temperature [°C]	Rate [°C/min]	Time [Min]
Evacuation	Helium	100	10	30
Evacuation	Helium	300	10	15
Evacuation		300	10	120
Leak test		300	10	-
Evacuation		300	10	60
Flow	Hydrogen	300	10	15
Analysis	Hydrogen	350	10	-

Table A10: Apparatus sequence of sorption measurements performed at 400°C.

Task	Gas	Temperature [°C]	Rate [°C/min]	Time [Min]
Evacuation	Helium	100	10	30
Evacuation	Helium	300	10	15
Evacuation		300	10	120
Leak test		300	10	-
Evacuation		300	10	60
Flow	Hydrogen	300	10	15
Analysis	Hydrogen	400	10	-

I Curve Fittings

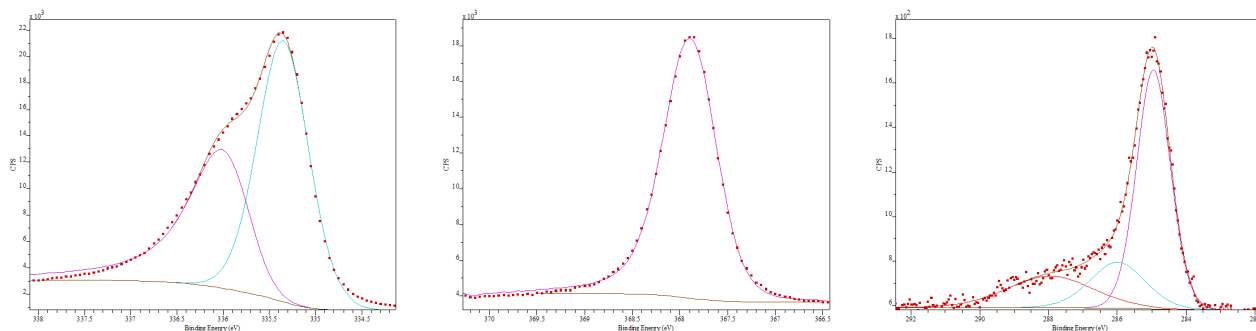


Figure A9: Curve fittings of Pd 3d, Ag 3d and C 1s on growth side of $10.0\mu\text{m}$ Pd/Ag membrane

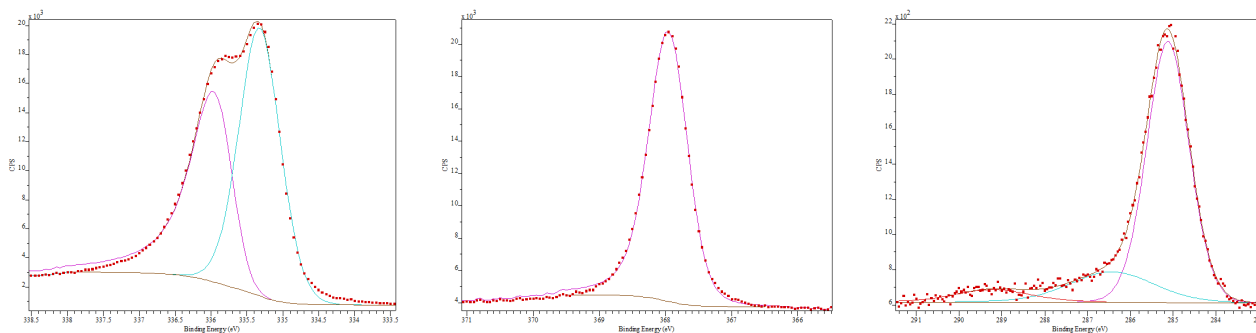


Figure A10: Curve fittings of Pd 3d, Ag 3d and C 1s on substrate side of $10.0\mu\text{m}$ Pd/Ag membrane

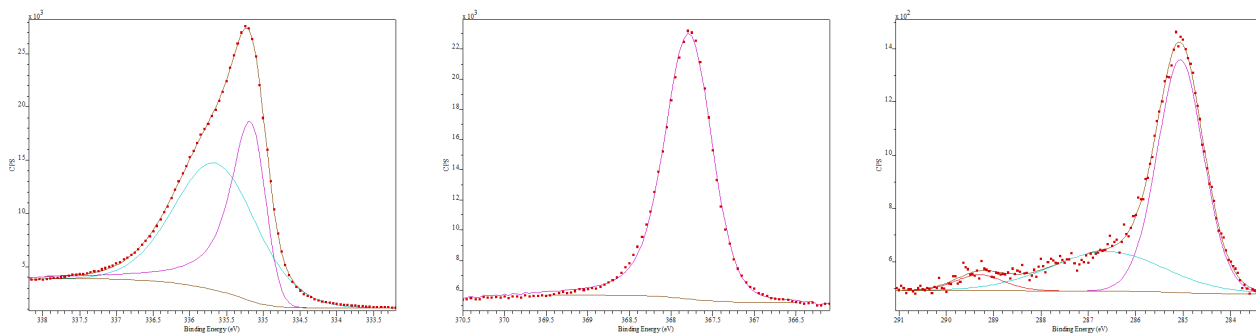


Figure A11: Curve fittings of Pd 3d, Ag 3d and C 1s on growth side of $2.2\mu\text{m}$ Pd/Ag membrane

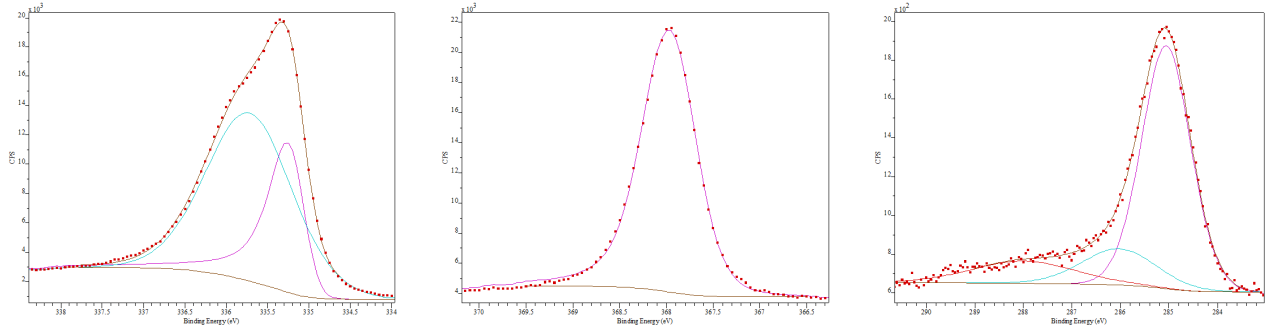


Figure A12: Curve fittings of Pd 3d, Ag 3d and C 1s on substrate side of 2.2 μm Pd/Ag membrane

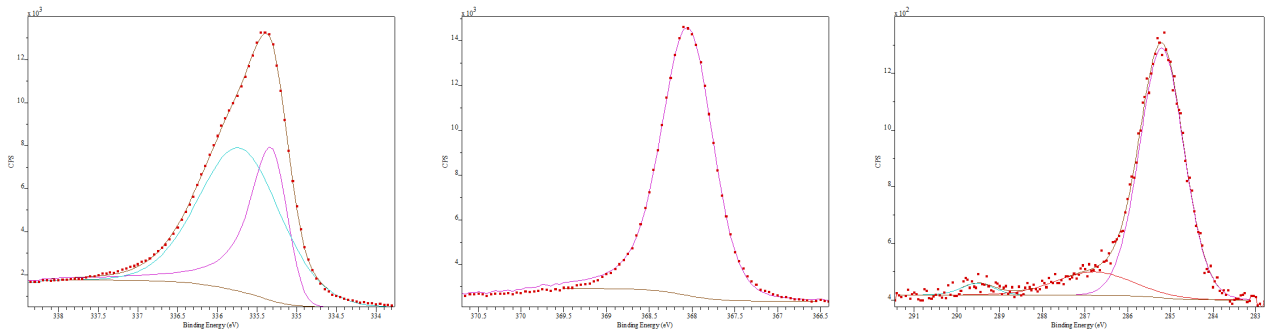


Figure A13: Curve fittings of Pd 3d, Ag 3d and C 1s on substrate side of 4.7 μm Pd/Ag membrane

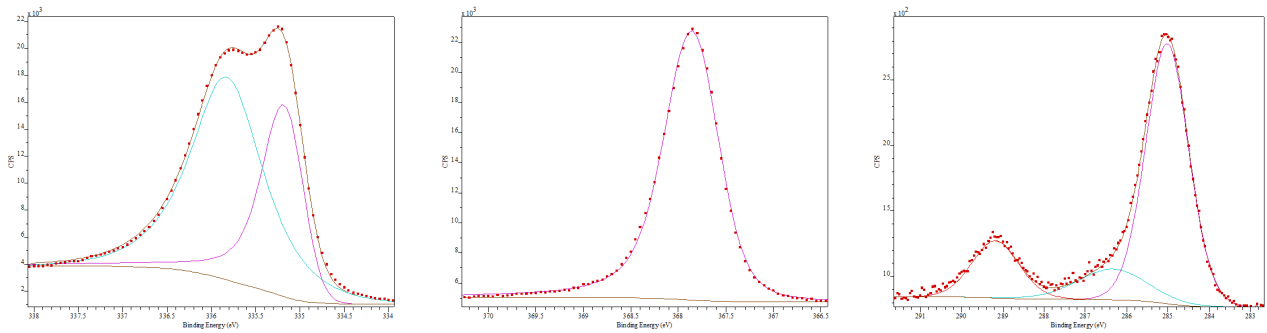


Figure A14: Curve fittings of Pd 3d, Ag 3d and C 1s on 4.7 μm Pd/Ag membrane from experiment 2a-3d

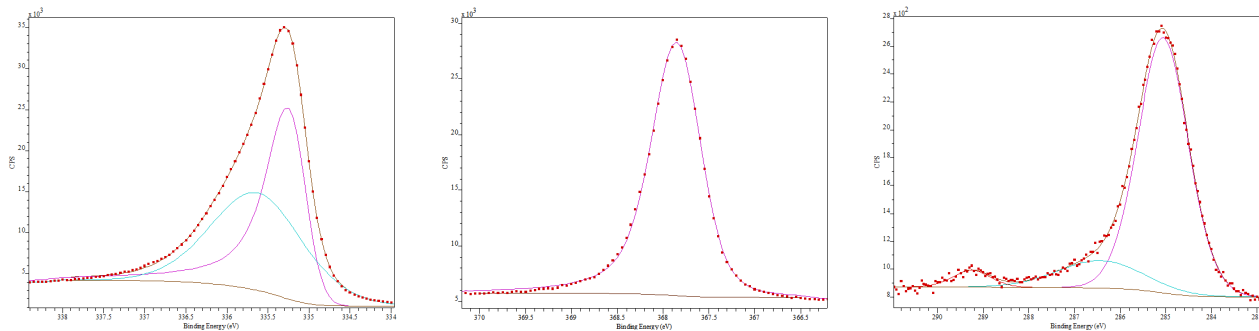


Figure A15: Curve fittings of Pd 3d, Ag 3d and C 1s on 4.7 μ m Pd/Ag membrane from experiment 4a-4f.

J Volumetric Hydrogen Adsorption Isotherms

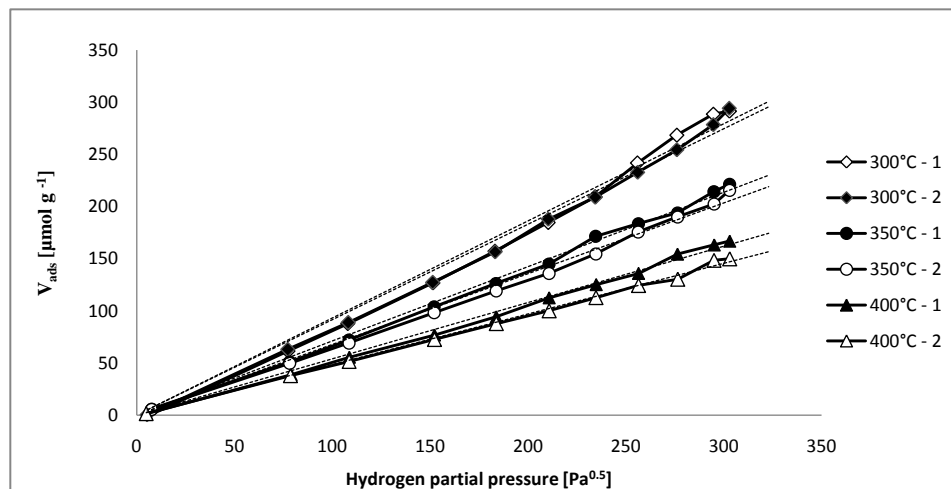


Figure A16: Volumetric adsorption of hydrogen as a function of hydrogen partial pressure for a $2.2\ \mu\text{m}$ Pd/Ag membrane at 300°C, 350°C and 400°C, with two parallels each. Linear trend lines for each plot are shown as stapled.

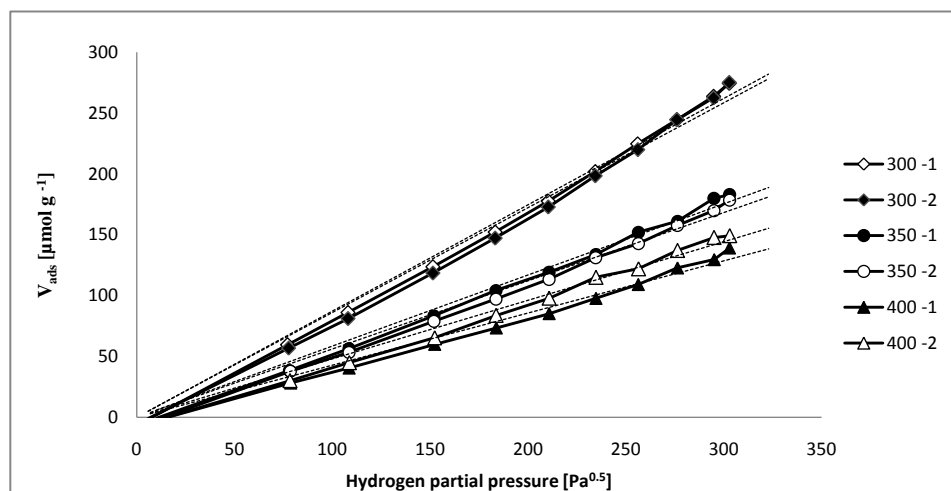


Figure A17: Volumetric adsorption of hydrogen as a function of hydrogen partial pressure for a $10.0\ \mu\text{m}$ Pd/Ag membrane at 300°C, 350°C and 400°C, with two parallels each. Linear trend lines for each plot are shown as stapled.

K Heat treatment effect before and after CO exposure

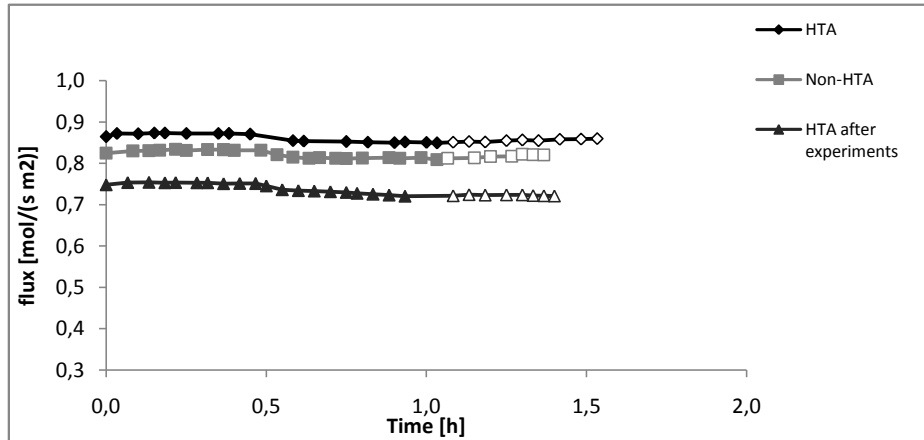


Figure A18: The flux as a function of time on stream at 0.5% CO exposure at 400°C, for heat treatment before and after experiment, as well as a membrane only stabilized in hydrogen. Hollow points indicates the regeneration phase where no *CO* is present.

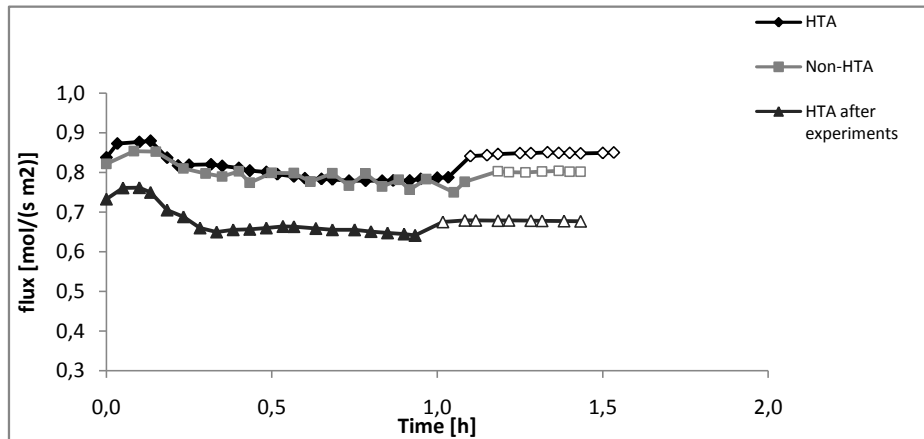


Figure A19: The flux as a function of time on stream at 2% CO exposure at 400°C, for heat treatment before and after experiment, as well as a membrane only stabilized in hydrogen. Hollow points indicates the regeneration phase where no *CO* is present.

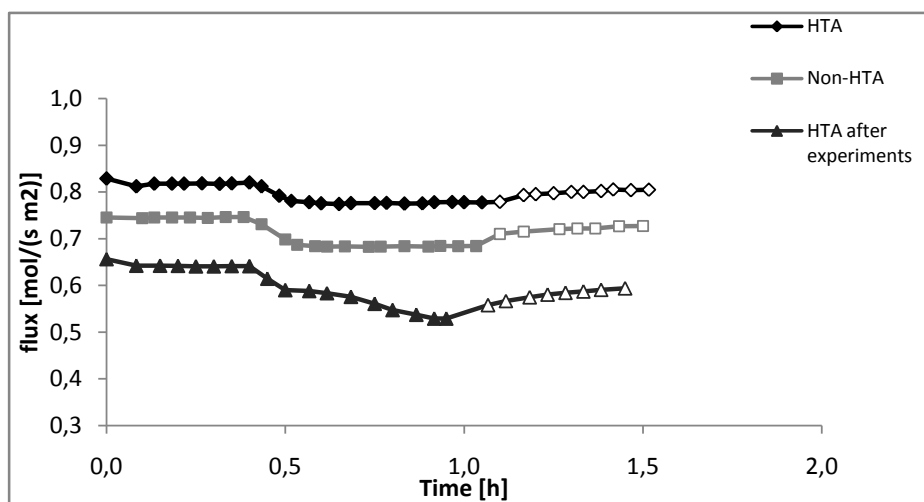


Figure A20: The flux as a function of time on stream at 0.5% CO exposure at 350°C, for heat treatment before and after experiment, as well as a membrane only stabilized in hydrogen. Hollow points indicates the regeneration phase where no CO is present.

L XPS Survey Spectra

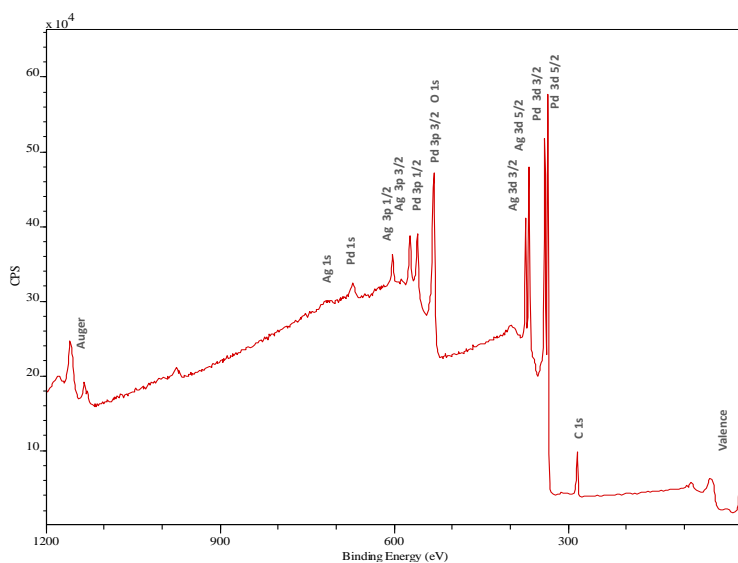


Figure A21: XPS Survey spectrum of unused growth side $2.2\mu\text{m}$ Pd/Ag membrane

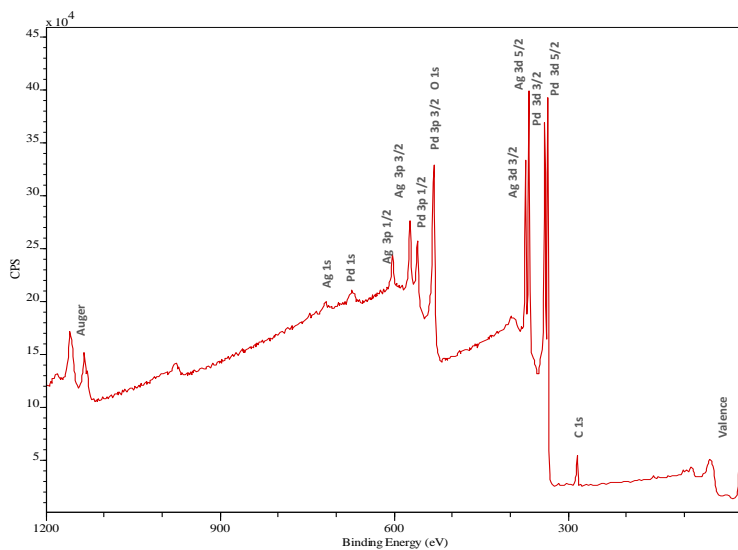


Figure A22: XPS Survey spectrum of unused substrate side $2.2\mu\text{m}$ Pd/Ag membrane

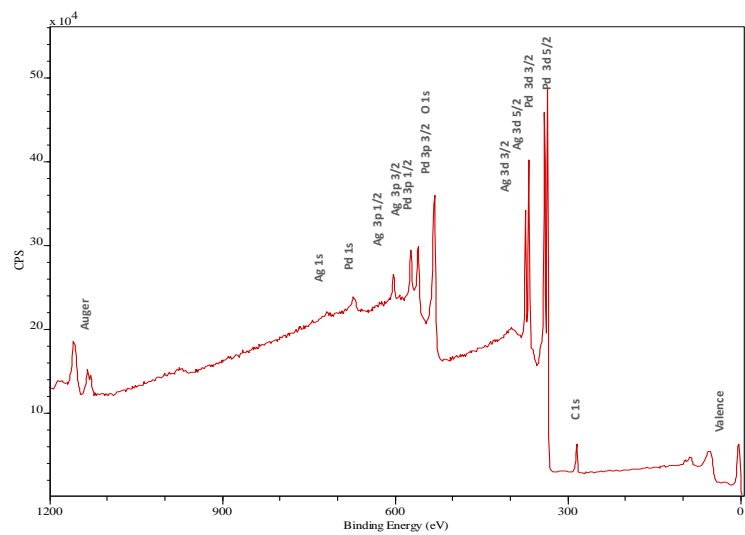


Figure A23: XPS Survey spectrum of unused growth side 2.2 μ m Pd/Ag membrane

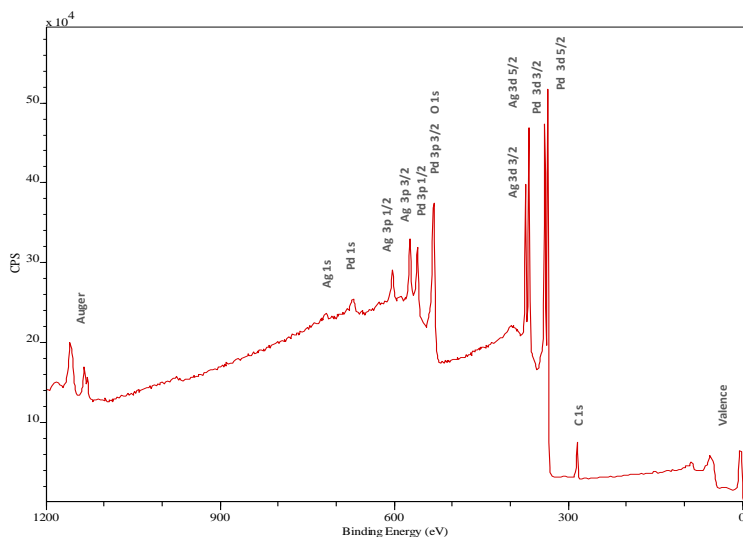


Figure A24: XPS Survey spectrum of unused substrate side 10.0 μ m Pd/Ag membrane